Ore Geology Reviews 153 (2023) 105297

Contents lists available at ScienceDirect

Ore Geology Reviews

journal homepage: www.elsevier.com/locate/oregeorev

Mineral associations and in-situ major and trace element compositions of dalyite from charoitites, Murun complex, Siberia

Emilia Yu. Dokuchits [a], Shao-Yong Jiang [a,*], Aleksandr S. Stepanov [a], Irina A. Zhukova [a], Tatiana A. Radomskaya [b], Hui-Min Su [a], Si-Qi Liu [a]

[a] State Key Laboratory of Geological Processes and Mineral Resources, Collaborative Innovation Center for Exploration of Strategic Mineral Resources, School of Earth Resources, China University of Geosciences, Wuhan 430074, China
[b] A.P. Vinogradov Institute of Geochemistry SB RAS, Irkutsk 664033, Russia

ARTICLE INFO

Keywords:
Zr–silicate, dalyite
In situ analysis
Geochemistry
Charoitites
Murun complex

ABSTRACT

The rare potassium Zr-silicate dalyite has been found in the charoitites of Murun alkaline complex as an accessory mineral and the main Zr phase. Electron probe microanalysis (EPMA) and laser ablation inductively coupled plasma mass spectrometry (LA-ICP-MS) were used to measure major and trace element compositions of dalyite, respectively. Dalyite from charoitites is defined by significant Ti ↔ Zr substitution and low extent of Na–K solid solution and mineral formula can be presented as $K_2(Zr_{1-x}Ti_x)Si_6O_{15}$. The Ti ↔ Zr substitution is a geothermometer in many minerals, however, the presence of zoning with increasing Ti from core towards the rim in dalyite from charoitites might indicate that element activity was more important factor than temperature. The first trace element analysis of dalyite shows that this mineral is enriched in lithophile elements, has strongly fractionated REE patterns but no Eu anomaly. Dalyite shares some common geochemical features with magmatic zircon: it shows HREE-enrichment and positive Ce anomaly relative to chondrite values, which could indicate that rare earth elements occur in similar structural position. Dalyite is an important mineral of peralkaline agpaitic rocks, a typical mineral of magmatic rocks, and likely indicates low-pressure conditions. Our new mineralogical and geochemical results on the dalyite clarify the role of Zr-silicates in agpaitic rocks and provide better understanding of the formation of charoitites.

1. Introduction

Zirconium is a key trace element in terrestrial rocks. In most rocks Zr is hosted by zircon, while in agpaitic alkaline rocks, complex Zr-silicates such as eudialyte, wadeite, dalyite, occur instead (Aja et al. 1996; Marks et al. 2011). Zr-silicates typically form as primary magmatic phases, however, they may also be products of hydrothermal alteration (Salvi and Williams-Jones 1995).

Dalyite is a rare triclinic silicate of Zr and K with the formula $K_2ZrSi_6O_{15}$. It was firstly described in peralkaline granites from Ascension Island by Van Tassel and Hey (1952). The crystal structure of dalyite was refined by Fleet (1965); it is a sheet silicate containing four, six- and eight-membered rings of SiO_4 tetrahedra. Dalyite had been discovered in several localities, for example, in peralkaline quartz syenites from São Miguel, Azores, Portugal (Cann 1967); in ultrapotassic volcanic rocks of Albacete Province, South-Eastern Spain (Linthout et al. 1988), in peralkaline, ultrapotassic syenite dykes, Western Norway (Furnes et al. 1982; Robins et al. 1983), and in aegirine-bearing albitite, South-Western Japan (Imaoka et al. 2021). A comprehensive summary on major element compositions of dalyite from different localities is available in Jeffery et al. (2016). In Russia, dalyite was found in two localities: as inclusions in eudialyte from quartz-microcline veins of the Lovozero complex (Ivanyuk et al. 2006), and in different rocks of the Sirenevyi Kamen charoite deposit in the Murun complex (Lazebnik and Makhotko 1982; Konev et al. 1996b). Murun alkaline complex is known for a wide variety of rare minerals, and many of them have been discovered within the complex (charoite, tinaksite, frankamenite, fluorcarletonite) (Rogov et al. 1965; Rogova et al. 1978; Lazebnik and Lazebnik 1981; Nikishova et al. 1996; Chakhmouradian et al. 2014; Kaneva et al. 2020). Zirconium-bearing minerals in Murun complex include: zircon [$Zr(SiO_4)$], wadeite [$K_2Zr(Si_3O_9)$] (Rogova and Sidorenko 1964), rosenbuschite [$Na_6Ca_6Zr_3Ti(Si_2O_7)_4O_2F_6$], eudialyte [$Na_{15}Ca_6Fe_3Zr_3Si(Si_{25}O_{73})(O,OH,H_2O)_3(Cl,OH)_2$], dalyite [$K_2ZrSi_6O_{15}$], and elpidite [$Na_2ZrSi_6O_{15}$*$3H_2O$] (Konev et al. 1996a). Accessory zircon was found in wide range of alkaline rocks of Murun complex (Dolivo-Dobrovolsky and

* Corresponding author.
E-mail address: shyjiang@cug.edu.cn (S.-Y. Jiang).

https://doi.org/10.1016/j.oregeorev.2023.105297
Received 30 September 2022; Accepted 6 January 2023
Available online 11 January 2023

Evdokimov 1991), however, in charoitites dalyite occurs instead of zircon. Lazebnik and Makhotko (1982) studied dalyite from fenite, carbonatite, charoitite, and aegirinite, and Konev et al. (1996b) found dalyite in charoitites of the southern part of Malyi Murun massif. A titanious-analogue of dalyite, named davanite, with the formula $K_2TiSi_6O_{15}$, was described in Lazebnik et al. (1984) in quartz-calcite-K-feldspar rocks from Murun complex.

In this study, we report representative EPMA major element and the first in situ LA–ICP–MS trace element dataset of dalyite in charoitites and discuss its compositional variation and the factors controlling the occurrence of dalyite.

2. Geological background

The Sirenevyi Kamen deposit of charoite is located in Murun complex, which is one of the most well-studied alkaline complexes of the Aldan shield. Murun complex consist of three major intrusions named Bolshoy Murun, Malyi Murun, and Dogaldynskii massifs (Konev et al. 1996a). Malyi Murun massif, which is commonly referred to as Murun complex, is the largest among them. The Malyi Murun pluton is a set of layered laccolite-like intrusions (Vorobiev 2008), located at the contact between the Riphean sediments of the platform cover and the Late Proterozoic basement rocks; it has elliptical shape, narrowing towards the northeast. Murun complex contains a wide range of rocks starting from ultramafic/mafic biotite pyroxenites and up to felsic granites and carbonatites, and this diversity is commonly attributed to intensive magmatic fractionation (Prokofiev and Vorobiev 1991; Mitchell et al. 1994; Panina and Usoltseva 2000; Vorobiev 2001; Vladykin and Tsaruk 2003; Vladykin, 2009; Vladykin, 2016). The $^{39}Ar/^{40}Ar$ dating gave Cretaceous ages of different intrusive facies and minerals from charoitites of Murun complex (Ivanov et al. 2018a; Ivanov et al., 2018b). The detailed geology of the Murun complex was described by Konev et al. (1996a) and Vorobiev (2008).

The Sirenevyi Kamen deposit was discovered by (Rogova et al. 1978), who proposed the hydrothermal metasomatic origin of these rocks. However, some researchers interpret charoitites as products of high-temperature magmatic crystallization (Vladykin et al. 1983; Prokofiev and Vorobiev 1991). In most publications charoitites were described as linear bodies hosted by fenites (Lazebnik and Lazebnik 1983; Borisov and Evdokimov 1984; Biryukov and Berdnikov 1993; Konev et al. 1996a). The petrography and mineralogy of rocks and minerals of the Murun complex were studied in numerous studies (e.g. Konev et al., 1996a; Vladykin et al., 1983; Vorobiev, 2008), however, petrography and geochemistry of Murun dalyite so far have received little attention.

3. Samples and analytical methods

This study was carried out on a set of samples of charoitites from the Murun Complex. The petrography was initially examined by reflected and transmitted light optical microscopy in thin sections using a Zeiss microscope. A JEOL JCM-7000 scanning electron microscope (SEM) at the Collaborative Innovation Center for Exploration of Strategic Mineral Resources, China University of Geosciences (Wuhan), was used for the examination of the polished thin sections of charoitites.

Major element compositions of dalyite from charoitites were analyzed by the electron microprobe with a JEOL JXA-8230 Electron Probe Microanalyzer (EPMA) equipped with five wavelength-dispersive spectrometers (WDS) at the Laboratory of Microscopy and Microanalysis, Wuhan Microbeam Analysis Technology Co., Ltd. Details of EPMA methods are described in Yang et al. (2022). The samples were coated with a thin conductive carbon coating prior to analysis. The procedures recommended by Zhang and Yang (2016) were used to minimize the difference of carbon film thickness between samples and obtain a ca. 20 nm uniform coating. Operating conditions for quantitative WDS analyses were as follows: an accelerating voltage of 15 kV, a beam current of 10nA and a 10 μm spot size. Data were corrected online using a ZAF (atomic number, absorption, fluorescence) correction procedure. The peak counting time was 10 s for Al, Fe, K, Mg, F, Na, Si, Ca, Zr, Sr, Ba and 20 s for Ti, Mn. The background counting time was 1/2 of the peak counting time on the high- and low-energy background positions. The following standards were used: pyrope (Fe), microcline (Si, Al, K), diopside (Ca, Mg), barium fluoride (F), jadeite (Na), zircon (Zr), rutile (Ti), rhodonite (Mn), barite (Ba), strontium fluoride (Sr) and hafnium (Hf). The 40 major element analyses of dalyite from seven samples of charoitites are given in the Table 1.

The major and trace element concentrations of minerals were determined by a NWR 193 HE laser ablation system with TwoVol3 cell coupled to an Agilent 7900 single quadrupole ICP mass spectrometer at the LA–ICP–MS laboratory in the Collaborative Innovation Center for Exploration of Strategic Mineral Resources, China University of Geosciences (Wuhan). The list of the analyzed isotopes included ^{7}Li, ^{9}Be, ^{11}B, ^{23}Na, ^{25}Mg, ^{27}Al, ^{29}Si, ^{31}P, ^{39}K, ^{42}Ca, ^{45}Sc, ^{47}Ti, ^{51}V, ^{53}Cr, ^{55}Mn, ^{57}Fe, ^{59}Co, ^{60}Ni, ^{63}Cu, ^{66}Zn, ^{71}Ga, ^{85}Rb, ^{88}Sr, ^{89}Y, ^{90}Zr, ^{93}Nb, ^{95}Mo, ^{133}Cs, ^{137}Ba, ^{139}La, ^{140}Ce, ^{141}Pr, ^{146}Nd, ^{147}Sm, ^{153}Eu, ^{157}Gd, ^{159}Tb, ^{163}Dy, ^{165}Ho, ^{166}Er, ^{169}Tm, ^{173}Yb, ^{175}Lu, ^{178}Hf, ^{181}Ta, ^{182}W, ^{208}Pb, ^{232}Th and ^{238}U. The ablation of the samples was performed using helium as the carrier gas that was mixed with Ar outside of the sample chamber. Each spot analysis incorporated approximately 30 s of background acquisition followed by 40 s data acquisition from the sample. A spot size of 32 μm (20 μm for thin rims of some dalyite crystals) was used together with a repetition rate of 8 Hz and an energy density of ~3.5 J cm^{-2}. Every 8–10 sample analyses were followed by several analyses of external reference materials. In this work, NIST SRM 610 was used as quality control (QC) reference material to correct the instrumental time-dependent sensitivity drift, and multiple external standards (NIST 610, NIST 612, BCR-2G, BHVO-2G and BIR-1G) were selectively used for external calibration (Liu et al. 2008). Silicon measured by EPMA for each analyzed spot was chosen as internal standard for calculation of the absolute concentrations. The time-resolved signals for each analyzed spot were carefully checked for presence of mineral inclusions. The off-line selection and integration of background and analyte signals, time drift correction and quantitative calibration were performed using both the ICPMSDataCal 10.9 software (Liu et al. 2008) and Iolite 4.0 software (with NIST 610 as a primary standard). Both ICPMSDataCal 10.9 and Iolite 4.0 had shown consistent results; here and after, we use the concentrations calculated by the ICPMSDataCal 10.9 software. The dataset of 24 trace element analyses of dalyite from eight samples is given in the Table 2.

4. Results

4.1. Petrography

4.1.1. Dalyite

Abundant dalyite was observed in three samples, and in fourteen samples tiny needle-like dalyite crystals were observed in small amounts. Dalyite associates with charoite, apatite, K-feldspar, pyroxene, tinaksite, strontianite, amphibole, and other minerals (Figs. 1-4). Dalyite usually occurs as a whitish-lilac or violet mineral with glassy luster, and in parallel polarized light a titaniferous variety is colorless (Konev et al. 1996b) (Fig. 2). In crossed polarized light, dalyite has high birefringence with bright colors distributed in spotted manner (Fig. 2). Konev et al. (1996b) proposed that whitish-violet color of dalyite could be related to small quantities of Ti^{3+}.

Dalyite forms anhedral feather-like (Fig. 2J–O) to isometric crystals (Fig. 2A–I). Isometric crystals are usually quite small (<50 μm), but in the samples cha-3–5 and MC-112 we found large crystals up to 200 μm with notable sectoral zoning evident on BSE images (Fig. 4A, B and D) and analyzed the cores and rims. Up to six zones in dalyite crystal could be observed (Fig. 4A and B), but the zones were narrow, and we could obtain four analyze across a crystal (Table 1); in most crystals only two data (core and rim) were obtained. Dalyite was also found in fibrous

Table 1
Representative EPMA analyses (wt.%) and atomic proportions (apfu) of dalyite.

No	1	2	3	4	5	6	7	8	9	10
Sample	cha-3–5	cha-3–5	cha-3–5	cha-3–5	cha-3–5	cha-3–5	cha-3–5	cha-3–5	cha-3–5	cha-3–5
Position	core	middle core	rim	core	middle core	rim	core	middle core	middle rim	rim
SiO_2	62.6	62.4	62.5	61.6	61.8	62.8	61.8	62.1	61.9	62.8
Al_2O_3	bdl	bdl	bdl	bdl	0.02	bdl	bdl	bdl	bdl	bdl
Na_2O	0.04	0.02	0.01	0.01	0.04	0.04	bdl	0.02	0.03	bdl
K_2O	15.2	15.8	15.9	15.8	15.7	16.1	15.8	15.8	15.9	16.0
CaO	0.01	bdl	bdl	bdl	0.01	bdl	bdl	bdl	bdl	bdl
ZrO_2	20.7	18.6	17.5	20.2	17.6	16.9	21.8	19.6	18.7	17.7
HfO_2	0.05	0.17	0.21	0.10	0.05	0.14	bdl	0.09	0.01	0.23
TiO_2	1.24	1.84	2.96	1.06	2.57	3.29	0.29	1.44	2.20	2.80
FeO	bdl	0.02	0.06	bdl	0.05	0.07	0.02	bdl	bdl	bdl
MnO	0.02	bdl	0.01	bdl	0.01	bdl	bdl	bdl	bdl	bdl
MgO	bdl	bdl	bdl	bdl	bdl	bdl	bdl	bdl	bdl	bdl
SrO	0.26	0.33	0.33	0.33	0.24	0.25	0.23	0.28	0.36	0.32
BaO	bdl	0.01	bdl	bdl	0.06	0.02	0.05	0.14	0.01	bdl
Total:	100	99.2	99.5	99.1	98.2	99.6	99.9	99.5	99.‘	99.8
Si	6.00	6.00	6.00	6.00	6.00	6.00	6.00	6.00	6.00	6.00
Al	bdl	bdl	bdl	bdl	bdl	bdl	bdl	bdl	bdl	bdl
Na	0.01	bdl	bdl	bdl	0.01	0.01	bdl	bdl	0.01	bdl
K	1.86	1.94	1.95	1.97	1.94	1.96	1.95	1.95	1.97	1.95
Ca	bdl	bdl	bdl	bdl	bdl	bdl	bdl	bdl	bdl	bdl
Zr	0.97	0.87	0.82	0.96	0.83	0.79	1.03	0.93	0.88	0.82
Hf	–	0.01	0.01	0.01	–	0.01	–	–	–	0.01
Ti	0.09	0.13	0.21	0.08	0.19	0.24	0.02	0.10	0.16	0.20
Fe	bdl	bdl	bdl	bdl	bdl	0.01	bdl	bdl	bdl	bdl
Mn	bdl	bdl	bdl	bdl	bdl	bdl	bdl	bdl	bdl	bdl
Mg	bdl	bdl	bdl	bdl	bdl	bdl	bdl	bdl	bdl	bdl
Sr	0,01	0,02	0,02	0,02	0,01	0,01	0,01	0,02	0,02	0,02
Ba	bdl	bdl	bdl	bdl	bdl	bdl	bdl	bdl	bdl	bdl

No	11	12	13	14	15	16	17	18	19	20
Sample	cha-3–5	cha-3–5	cha-3–5	cha-3–5	cha-1–1	cha-1–1	cha-1–1	cha-1–1	cha-1–1	cha-1–1
Position	core	middle core	middle rim	rim	core	rim	core	rim	core	rim
SiO_2	61.4	62.1	62.4	62.7	61.8	62.4	62.2	61.6	62.0	62.8
Al_2O_3	bdl	bdl	bdl	bdl	0.01	bdl	0.01	bdl	bdl	0.01
Na_2O	0.02	bdl	0.01	bdl	0.01	0.05	0.01	bdl	0.05	0.01
K_2O	15.5	15.9	15.8	16.1	15.6	15.7	15.9	15.8	15.6	16.4
CaO	bdl	bdl	bdl	bdl	0.01	bdl	bdl	bdl	bdl	0.02
ZrO_2	19.9	20.4	19.5	16.6	20.2	19.1	18.9	20.9	19.4	18.2
HfO_2	0.33	0.05	0.09	0.12	bdl	0.24	0.20	0.21	bdl	0.10
TiO_2	1.36	0.97	1.69	3.34	0.74	1.57	1.07	0.88	0.84	1.32
FeO	0.02	bdl	0.03	0.06	bdl	0.09	bdl	0.04	0.02	bdl
MnO	0.02	0.02	bdl	bdl	bdl	bdl	bdl	bdl	0.04	bdl
MgO	bdl	bdl	bdl	bdl	bdl	bdl	bdl	bdl	bdl	bdl
SrO	0.32	0.24	0.34	0.26	0.31	0.31	0.33	0.31	0.40	0.37
BaO	0.03	0.12	0.04	0.07	bdl	0.03	0.03	bdl	0.04	0.05
Total:	98.9	99.8	99.9	99.3	98.7	99.5	98.6	99.8	98.4	99.4
Si	6.00	6.00	6.00	6.00	6.00	6.00	6.00	6.00	6.00	6.00
Al	bdl	bdl	bdl	bdl	bdl	bdl	bdl	bdl	bdl	bdl
Na	bdl	bdl	bdl	bdl	bdl	0.01	bdl	bdl	0.01	bdl
K	1.93	1.96	1.93	1.96	1.94	1.92	1.96	1.96	1.92	2.00
Ca	bdl	bdl	bdl	bdl	bdl	bdl	bdl	bdl	bdl	bdl
Zr	0.95	0.96	0.92	0.78	0.96	0.90	0.89	0.99	0.92	0.85
Hf	0.02	bdl	bdl	0.01	bdl	0.01	0.01	0.01	bdl	0.01
Ti	0.10	0.07	0.12	0.24	0.05	0.11	0.08	0.06	0.06	0.09
Fe	bdl	bdl	bdl	bdl	bdl	0.01	bdl	bdl	bdl	bdl
Mn	bdl	bdl	bdl	bdl	bdl	bdl	bdl	bdl	bdl	bdl
Mg	bdl	bdl	bdl	bdl	bdl	bdl	bdl	bdl	bdl	bdl
Sr	0.02	0.01	0.02	0.01	0.02	0.02	0.02	0.02	0.02	0.02
Ba	bdl	bdl	bdl	bdl	bdl	bdl	bdl	bdl	bdl	bdl

	21	22	23	24	25	26	27	28	29	30
Sample	cha-1–1	cha-1–1	MC-112	MC-112	MC-112	MC-112	MC-112	MC-112	MC-112	MC-112
Position	core	rim	core	rim	core	rim	core	rim	core	rim
SiO_2	61.7	61.6	61.7	62.3	62.0	62.4	62.2	62.0	61.9	62.4
Al_2O_3	0.01	bdl	0.01	0.02	bdl	bdl	bdl	bdl	bdl	bdl
Na_2O	bdl	0.02	bdl	0.01	bdl	0.02	0.02	0.01	bdl	0.01
K_2O	15.8	15.7	15.9	15.9	15.9	16.2	15.8	15.8	15.8	16.0
CaO	bdl	bdl	bdl	bdl	bdl	bdl	bdl	bdl	bdl	bdl
ZrO_2	20.6	21.3	19.6	17.8	19.3	17.5	19.8	18.8	19.2	18.9

(*continued on next page*)

Table 1 (*continued*)

	21	22	23	24	25	26	27	28	29	30
Sample	cha-1–1	cha-1–1	MC-112	MC-112	MC-112	MC-112	MC-112	MC-112	MC-112	MC-112
Position	core	rim	core	rim	core	rim	core	rim	core	rim
HfO_2	0.08	bdl	0.28	0.26	0.15	0.11	0.25	0.36	0.19	0.15
TiO_2	0.76	0.52	1.66	2.41	1.54	2.83	1.20	1.72	1.71	2.06
FeO	0.02	bdl	0.03	0.06	0.03	0.05	0.07	bdl	0.03	bdl
MnO	bdl	bdl	0.02	bdl	bdl	bdl	bdl	bdl	bdl	bdl
MgO	bdl	bdl	bdl	bdl	bdl	bdl	bdl	bdl	bdl	bdl
SrO	0.40	0.34	0.25	0.22	0.29	0.38	0.19	0.34	0.26	0.33
BaO	0.02	0.11	0.02	0.01	0.08	bdl	0.11	bdl	0.01	0.09
Total:	99.4	99.6	99.4	99.0	99.2	99.0	99.6	99.0	99.0	100
Si	6.00	6.00	6.00	6.00	6.00	6.00	6.00	6.00	6.00	6.00
Al	bdl	bdl	bdl	bdl	bdl	bdl	bdl	bdl	bdl	bdl
Na	bdl	bdl	bdl	bdl	bdl	bdl	bdl	bdl	bdl	bdl
K	1.96	1.95	1.97	1.95	1.96	1.99	1.94	1.95	1.95	1.97
Ca	bdl	bdl	bdl	bdl	bdl	bdl	bdl	bdl	bdl	bdl
Zr	0.98	1.01	0.93	0.84	0.91	0.80	0.93	0.89	0.91	0.88
Hf	–	–	0.02	0.01	0.01	0.01	0.01	0.02	0.01	0.01
Ti	0.06	0.04	0.12	0.17	0.11	0.20	0.09	0.13	0.12	0.15
Fe	bdl	bdl	bdl	bdl	bdl	bdl	0.01	bdl	bdl	bdl
Mn	bdl	bdl	bdl	bdl	bdl	bdl	bdl	bdl	bdl	bdl
Mg	bdl	bdl	bdl	bdl	bdl	bdl	bdl	bdl	bdl	bdl
Sr	0.02	0.02	0.01	0.01	0.02	0.02	0.01	0.02	0.01	0.02
Ba	bdl	bdl	bdl	bdl	bdl	bdl	bdl	bdl	bdl	bdl

No	31	32	33	34	35	36	37	38	39	40	Average	σ
Sample	MC-112	MC-112	MC-112	MC-112	MC-112	MC-112	MC-112	MC-112	MC-112	MC-112		
Position	middle core	rim	core	rim	core	rim	core	rim	core	rim		
SiO_2	61.5	62.0	62.3	62.6	61.9	62.3	61.8	61.9	61.8	62.5	62.1	0.39
Al_2O_3	bdl	0.02	0.03	0.01	bdl	0.02	bdl	0.02	bdl	bdl	–	0.01
Na_2O	0.03	bdl	0.02	0.02	0.04	0.05	0.02	0.02	bdl	bdl	0.02	0.02
K_2O	15.9	16.1	15.8	15.9	15.9	15.9	15.8	15.8	15.8	15.9	15.8	0.20
CaO	bdl	0.01	bdl	0.01	bdl	bdl	0.01	bdl	bdl	bdl	–	–
ZrO_2	19.2	16.8	19.6	18.0	20.5	19.2	20.3	17.7	19.5	17.4	19.1	1.31
HfO_2	0.19	0.04	0.29	0.26	0.07	0.32	0.17	0.19	0.22	0.34	0.16	0.10
TiO_2	1.65	2.91	1.27	2.66	0.85	1.74	1.06	2.75	1.27	2.72	1.72	0.81
FeO	0.05	0.03	bdl	0.01	bdl	bdl	0.01	0.02	bdl	0.03	0.02	0.02
MnO	0.03	bdl	0.01	bdl	0.05	bdl	0.02	bdl	bdl	0.02	0.01	0.01
MgO	bdl	bdl	bdl	bdl	bdl	bdl	bdl	bdl	bdl	bdl	–	–
SrO	0.28	0.29	0.30	0.37	0.32	0.25	0.28	0.25	0.30	0.25	0.30	0.05
BaO	bdl	0.09	bdl	0.04	bdl	0.11	bdl	0.06	0.03	0.13	0.04	0.04
Total:	98.9	98.3	99.6	100	99.6	100	99.5	98.7	98.8	99.4	99.3	0.49
Si	6.00	6.00	6.00	6.00	6.00	6.00	6.00	6.00	6.00	6.00	6.00	–
Al	bdl	bdl	bdl	bdl	bdl	bdl	bdl	bdl	bdl	bdl	–	–
Na	0.01	bdl	bdl	bdl	0.01	0.01	bdl	bdl	bdl	bdl	–	–
K	1.98	1.98	1.94	1.95	1.96	1.96	1.95	1.95	1.95	1.95	1.95	0.02
Ca	bdl	bdl	bdl	bdl	bdl	bdl	bdl	bdl	bdl	bdl	–	–
Zr	0.91	0.79	0.92	0.84	0.97	0.90	0.96	0.84	0.92	0.81	0.90	0.07
Hf	0.01	bdl	0.02	0.01	bdl	0.02	0.01	0.01	0.01	0.02	0.01	0.01
Ti	0.12	0.21	0.09	0.19	0.06	0.13	0.08	0.20	0.09	0.20	0.12	0.06
Fe	bdl	bdl	bdl	bdl	bdl	bdl	bdl	bdl	bdl	bdl	–	–
Mn	bdl	bdl	bdl	bdl	bdl	bdl	bdl	bdl	bdl	bdl	–	–
Mg	bdl	bdl	bdl	bdl	bdl	bdl	bdl	bdl	bdl	bdl	–	–
Sr	0.02	0.02	0.02	0.02	0.02	0.01	0.02	0.01	0.02	0.01	0.02	–
Ba	bdl	bdl	bdl	bdl	bdl	bdl	bdl	bdl	bdl	bdl	–	–

Atoms Per Formula Unit calculated on the basis of 6 atoms of Si.
Note. dash means no data; bdl means below detection limit.

charoite, forming feather-like grains often cut by needles of charoite and intergrown with apatite, K-feldspar, strontianite, barytocalcite, and other minerals (Fig. 2J–R).

Close association of dalyite with tiny grains of Sr- and Ba-bearing carbonate minerals have been observed in all the studied samples, and the presence of carbonate micro inclusions in dalyite complicated the analysis. During petrographic study of the sample cha-1–1, we observed abundant fluid and mineral inclusions trapped in dalyite (Fig. 5), which were randomly distributed within the grain. Due to decrepitation within the range 192–300 °C we couldn't measure the homogenization temperatures of inclusions, and additional study on this topic is desirable. We tried to avoid visible inclusions during the LA–ICP–MS analytical process and filtered out the analyses affected by impurities.

4.1.2. Wadeite

We found wadeite in the sample cha-1–1 in a form of 5–50 μm mineral inclusions in dalyite crystals (up to 500 μm) (Fig. 3E and F). The texture suggests that wadeite formed first and was then replaced by dalyite. Previously, wadeite has been described as accessory mineral in syenite (Rogova and Sidorenko 1964; Reguir 2001) and fenite (Konev et al. 1996a) of the Murun complex and apparently, this is the first observation of wadeite in charoitites.

4.1.3. Charoite

Charoite is a main rock forming mineral of charoitites. Most often we observed dalyite in the samples of charoitite with banded-fibrous (Fig. 1A) or "rosette-like" textures. Needle-like charoite often observed

Table 2
Representative LA-ICP-MS analyses for trace and rare earth element concentrations of dalyite (ppm).

No	1	2	3	4	5	6	7	8	9	10	11	12	13
Sample	cha-3–5	cha-3–5	cha-3–5	cha-3–5	cha-3–5	cha-3–5	cha-3–5	cha-3–5	cha-3–5	cha-3–5	cha-3–5	cha-3–5	cha-3–5
Position	core	core	core	core	core	rim	core	rim	core	rim	middle rim	core	core
Li	11.5	4.25	bdl	0.11	bdl	bdl	0.77	bdl	bdl	bdl	bdl	bdl	0.12
Be	2.44	bdl	0.87	0.89	bdl	0.46	bdl	bdl	0.46	1.02	0.44	0.01	bdl
B	22.0	39.5	0.91	1.34	2.79	4.88	3.49	0.17	4.45	0.28	0.09	3.66	0.82
Na	107	91	95.2	102	71.5	74.7	102	68.1	59.0	102	68.6	84.6	197
Mg	0.75	2.94	2.01	1.23	0.73	2.25	1.27	1.27	2.11	1.21	0.40	1.72	5.59
Al	2.13	3.24	0.15	3.91	2.86	2.92	3.05	3.44	2.62	1.73	2.70	2.26	5.05
P	bdl	bdl	10.8	21.9	41.1	bdl	8.29	22.3	6.82	17.7	36.7	80.5	32.8
Ca	117	123	bdl	bdl	bdl	bdl	16.4	bdl	bdl	226	227	33.5	368
Sc	33.9	36.4	66.8	69.4	71.1	62.9	69.0	59.1	67.4	58.0	59.4	61.8	69.4
Ti	9033	8421	8926	8004	9253	12,106	9095	13,380	9233	12,459	13,329	8407	8992
V	16.6	13.3	25.2	26.3	43.2	26.2	25.0	28.4	16.8	35.6	31.7	8.63	24.4
Cr	4.18	0.53	18.8	4.35	11.2	7.81	4.69	5.11	3.06	10.6	2.12	0.62	2.36
Mn	bdl	0.05	0.90	1.34	0.29	1.35	0.88	1.05	0.21	0.89	bdl	0.69	1.87
Fe^{2+}	73	76	108	101	128	121	83.0	140	87.2	128	110	73.7	241
Co	bdl	0.03	bdl	bdl	0.02	0.05	0.06	bdl	0.06	bdl	bdl	0.20	bdl
Ni	1.12	0.07	0.83	1.06	0.82	1.26	0.67	0.33	bdl	0.16	1.45	bdl	bdl
Cu	0.16	0.48	0.23	0.08	bdl	bdl	bdl	0.02	0.13	0.25	0.13	0.08	0.15
Zn	0.30	bdl	0.81	0.93	0.27	1.13	0.44	1.47	0.12	0.29	0.50	bdl	0.14
Ga	bdl	0.02	bdl	1.62	0.05	bdl	0.04	0.01	0.13	bdl	0.37	bdl	0.07
Ge	bdl	0.13	0.01	0.14	bdl	bdl	bdl	0.26	0.13	bdl	0.50	0.70	bdl
Rb	410	408	414	417	417	417	420	411	419	410	423	411	418
Sr	0.59	0.53	0.65	0.68	0.88	0.88	1.01	0.85	0.53	0.79	0.56	0.58	4.25
Y	20.7	23.3	5.02	15.0	5.70	16.4	21.6	8.30	19.1	5.73	4.55	35.4	17.8
Zr	149,589	146,967	160,005	157,008	159,442	149,352	156,307	146,513	153,482	147,643	147,668	153,090	151,886
Nb	2.62	3.05	1.53	6.74	1.24	1.83	2.02	2.14	2.60	1.29	2,04	3,89	2,85
Cd	6.15	6.86	9.52	7.83	8.43	7.19	7.75	6.01	9.48	bdl	0,11	0,60	9,96
Sn	147	89.4	230	158	61.9	219	117	239	141	236	259	116	93,6
Cs	1.78	1.57	2.33	2.24	2.21	1.53	2.16	1.66	1.73	1.89	1.45	1.26	2.14
Ba	214	216	227	238	333	289	283	286	228	305	270	210	252
La	0.02	0.01	bdl	0.03	bdl	0.01	0.02	0.03	bdl	bdl	0.02	0.02	0.02
Ce	2.26	2.43	1.63	1.15	1.42	2.51	2.06	2.68	2.54	2.02	1.88	2.91	1.65
Pr	0.04	0.01	0.01	0.02	0.01	0.02	0.01	0.02	0.01	0.02	0.01	0.02	0.03
Nd	0.05	0.12	0.06	bdl	0.06	0.11	0.07	0.05	0.10	0.05	0.28	0.07	0.09
Sm	0.08	0.06	0.07	0.04	bdl	0.15	0.06	0.04	0.02	0.03	0.11	0.14	0.05
Eu	0.05	0.06	0.02	0.03	0.01	0.06	0.03	0.02	0.08	0.02	0.02	0.09	0.03
Gd	0.11	0.25	0.05	0.08	0.12	0.28	0.29	0.19	0.26	0.07	0.19	0.48	0.15
Tb	0.09	0.13	0.02	0.05	0.04	0.06	0.13	0.06	0.10	0.03	0.03	0.15	0.08
Dy	1.23	1.51	0.24	0.78	0.38	0.97	1.36	0.58	1.22	0.30	0.27	2.21	1.13
Ho	0.48	0.67	0.11	0.35	0.15	0.44	0.58	0.22	0.50	0.17	0.12	0.93	0.47
Er	2.76	3.24	0.68	2.33	1.14	2.37	3.06	1.04	2.61	0.80	0.68	4.92	2.57
Tm	0.64	0.91	0.25	0.71	0.35	0.57	0.81	0.30	0.71	0.15	0.15	1.25	0.78
Yb	8.12	8.61	2.39	7.56	3.86	6.25	9.12	2.87	7.35	2.11	1.62	12.8	8.60
Lu	1.58	1.82	0.51	1.57	0.89	1.19	2.09	0.54	1.47	0.52	0.37	2.46	1.71
Hf	1085	891	943	828	817	891	815	883	822	948	908	851	835
Ta	0.43	0.39	0.14	0.19	0.10	0.38	0.29	0.41	0.59	0.26	0.39	0.51	0.49
Pb	0.97	0.36	bdl	0.57	0.65	0.48	0.51	2.30	0.37	bdl	bdl	0.42	0.54
Th	4.32	3.46	8.49	11.7	6.56	4.28	5.24	5.21	3.22	4.38	4.65	2.21	7.58
U	266	305	354	467	265	219	275	198	378	149	168	311	524
∑ REE	17.4	19.8	6.06	14.7	8.42	15.0	19.7	8.63	17.0	6.27	5.76	28.4	17.4

No	14	15	16	17	18	19	20	21	22	23	24	Average	σ	Detection limit
Sample Position	cha-3–5 middle rim	cha-3–5 core	cha-3–5 rim	cha-3–5 core	cha-1–1 core	cha-1–1 core	cha-1–1 core	cha-1–1 core	MC-112 core	MC-112 core	MC-112 core			
Li	bdl	9.59	bdl	0.58	0.57	bdl	bdl	bdl	0.33	0.21	bdl	0.85	2.18	3.27
Be	0.08	bdl	0.82	0.12	0.57	0.40	0.28	0.88	bdl	0.47	bdl	0.45	0.60	1.09
B	3.09	bdl	8.87	bdl	0.71	1.70	2.29	2.85	1.93	0.85	2.93	3.98	8.19	6.47
Na	60.5	57.2	88.4	89.6	94.7	134	64.2	96.9	74.1	96.5	113	90.1	29.4	-*
Mg	2.20	3.15	2.60	2.01	1.14	1.03	0.97	1.02	1.68	2.35	2.58	1.81	1.13	-*
Al	3.72	8.43	4.24	3.69	16.1	14.9	29.0	10.0	4.64	4.24	5.02	5.78	6.31	-*
P	25.3	66.3	99.0	bdl	60.7	bdl	26.8	bdl	bdl	bdl	45.2	31.5	27.5	0.02
Ca	bdl	bdl	bdl	475	bdl	bdl	41.8	145	bdl	bdl	bdl	181	216	0.07
Sc	58.2	97.5	60.3	59.0	57.7	58.6	59.8	61.1	57.8	55.8	57.0	61.0	12.0	0.17
Ti	12,528	6069	10,737	9743	6976	7444	7584	5475	14,125	13,379	11,458	9977	2524	-*
V	22.1	23.9	12.5	13.6	34.9	38.1	31.9	27.4	23.1	21.2	18.1	24.7	8.52	0.14
Cr	1.48	2.43	3.90	4.51	2.50	6.38	75.4	bdl	3.88	2.19	3.08	7.44	15.1	3.03
Mn	bdl	bdl	bdl	1.57	2.38	0.57	bdl	0.24	0.18	bdl	1.06	0.87	0.65	-*
Fe^{2+}	139	69.4	61.1	43.7	343	391	357	274	183	180	131	154	97.5	-*
Co	0.09	bdl	bdl	0.01	bdl	0.08	0.03	bdl	0.09	0.02	bdl	0.04	0.05	0.12
Ni	1.43	bdl	bdl	4.71	1.35	bdl	bdl	bdl	1.07	0.37	3.71	1.34	1.83	4.18
Cu	bdl	0.79	1.08	bdl	0.34	bdl	bdl	bdl	0.16	bdl	0.05	0.19	0.30	0.55

(*continued on next page*)

Table 2 (*continued*)

No	14	15	16	17	18	19	20	21	22	23	24	Average	σ	Detection limit
Sample	cha-3–5	cha-3–5	cha-3–5	cha-3–5	cha-1–1	cha-1–1	cha-1–1	cha-1–1	MC-112	MC-112	MC-112			
Position	middle rim	core	rim	core	core	core	core	core	core	core	core			
Zn	0.46	0.99	1.43	1.34	bdl	0.19	bdl	0.39	0.12	bdl	0.86	0.45	0.48	1.13
Ga	bdl	bdl	0.44	bdl	bdl	bdl	bdl	0.25	bdl	0.33	bdl	0.19	0.37	1.08
Ge	0.49	bdl	2.10	bdl	bdl	bdl	bdl	0.01	0.46	0.24	0.24	0.27	0.46	1.19
Rb	415	435	420	412	425	425	432	438	410	411	405	418	8.37	0.59
Sr	1.52	2.37	5.42	0.63	2.13	2.86	2.32	2.29	2.77	1.59	1.99	30.5	64.2	0.09
Y	14.7	13.7	25.9	27.3	47.5	46.8	41.7	51.8	1.03	1.15	1.36	17.9	18.6	0.01
Zr	143,622	159,070	150,312	152,078	155,736	158,062	150,556	156,678	145,761	145,309	144,337	150,340	5788	0.31
Nb	2,33	17,7	3,29	3,01	50,2	45,0	54,4	37.5	0.94	1.05	1.09	12.5	24.3	–
Cd	bdl	0,92	0,17	0,25	0,03	bdl	0,07	5.21	5.28	5.94	5.23	6.09	1.69	0.68
Sn	145	115	150	115	1012	1016	1036	938	982	988	925	474	397	0.95
Cs	1.59	2.38	1.41	1.83	2.17	1.98	2.02	2.47	1.50	1.78	1.79	1.89	0.36	0.12
Ba	269	215	242	215	480	497	396	384	292	287	348	306	82.5	0.10
La	0.02	0.04	0.02	bdl	0.03	0.06	0.03	0.02	0.01	0.01	0.01	0.17	0.32	–
Ce	2.34	0.79	3.19	2.49	4.23	4.27	3.96	4.08	2.20	2.05	1.85	2.77	1.13	–
Pr	0.01	0.01	0.04	bdl	0.06	0.05	0.06	0.06	0.02	0.03	0.02	0.07	0.09	–
Nd	0.11	bdl	0.14	0.10	0.50	0.35	0.28	0.41	0.15	0.14	0.13	0.32	0.32	0.01
Sm	0.04	0.28	0.11	0.28	0.38	0.22	0.28	0.25	0.05	0.05	0.08	0.15	0.13	0.01
Eu	0.05	bdl	0.06	0.05	0.19	0.20	0.10	0.20	0.01	0.01	0.01	0.06	0.06	0.01
Gd	0.37	0.26	0.20	0.36	1.06	0.97	0.79	0.86	0.04	0.05	0.10	0.33	0.44	0.02
Tb	0.06	0.09	0.22	0.12	0.28	0.31	0.26	0.31	0.01	0.01	0.02	0.10	0.12	–
Dy	0.80	0.82	2.20	1.98	3.25	3.21	2.62	3.95	0.13	0.15	0.17	1.19	1.29	0.01
Ho	0.35	0.36	0.74	0.69	1.20	1.17	0.99	1.36	0.03	0.03	0.02	0.45	0.46	–
Er	2.16	2.26	3.51	3.38	6.57	6.67	5.46	6.65	0.07	0.09	0.13	2.43	2.46	–
Tm	0.52	0.71	0.96	0.97	1.91	1.81	1.57	1.90	0.03	0.03	0.01	0.67	0.66	–
Yb	5.78	7.42	9.72	9.63	19.8	20.3	18.9	21.1	0.22	0.23	0.37	7.16	7.06	0.02
Lu	1.16	1.85	1.90	2.08	4.66	4.27	4.17	4.82	0.06	0.05	0.09	1.54	1.51	–
Hf	811	922	834	843	798	827	799	812	1648	1646	1248	1016	343	–
Ta	0.44	0.14	0.51	0.41	3.12	3.02	3.23	2.30	0.15	0.19	0.12	0.69	0.93	–
Pb	bdl	0.37	0.48	0.23	2.02	2.26	1.88	1.75	0.70	0.73	bdl	1.08	0.79	0.10
Th	3.86	17.3	2.56	2.74	46.2	39.2	43.9	51.8	5.66	7.64	6.05	15.3	25.0	0.01
U	270	655	363	253	359	324	317	360	72.8	73.2	74.8	282	156	–
∑ REE	13.8	14.9	23.0	22.1	44.2	43.8	39.5	46.0	3.05	2.94	3.02	17.4	14.6	

Note. bdl means below detection limit.
Dash means detection limit is 0.
* Detection limit is shown for oxide.

in close intergrowth with crystals of dalyite, cutting these crystals (Fig. 2J–R). Charoite formed at the later stage in sample MC-112, where dalyite was brecciated and cemented by charoite fine-grained mass (Fig. 1B, Fig. 2A–C). In cha-1–1 and cha-3–5, dalyite forms fine-grained isometric or slightly elongated crystals, overgrown by charoite (Fig. 2D–I).

4.1.4. K-feldspar

K-feldspar is a common rock-forming mineral of charoitites, it was observed in all the samples with dalyite (Fig. 1A and B; Fig. 2C–F; Fig. 3G and H). We observed several generations of K-feldspar: one generation of K-feldspar is represented by tabular coarse K-feldspar grains (Fig. 3G) or fine-grained aggregates, associated with dalyite, apatite and pyroxene (Fig. 3H and D). Late generation of K-feldspar also can be formed by coarse and fine grains, and usually associates with charoite, forming band-like layered texture (Fig. 3H).

4.1.5. Fluorapatite

Fluorapatite is widespread in charoitites, and often closely associates with dalyite (Fig. 2D–F, J–O; Fig. 3A, C and H). It usually forms anhedral (20–500 μm in size) grains and found as inclusions in many minerals of charoitites. We observed fluorapatite hosted in charoite, amphibole, K-feldspar, tinaksite, fedorite, frankamenite. This mineral in charoitites often host large amount of fluid inclusions.

4.1.6. Pyroxene

Pyroxene in charoitites is represented by idiomorphic and hypidiomorphic crystals of dark green aegirine. It was observed among dalyite crystals (Fig. 1A; Fig. 2I; Fig. 3C–E). Same as dalyite, pyroxene from charoitites often demonstrates chemical zoning. Aegirine, as well as tinaksite, often forms spherulitic aggregates.

4.1.7. Quartz

Quartz is a common rock-forming mineral in charoitites. It forms large coarse grains, as well as fine grains and late thin veins (Fig. 3B and C) and present in all samples with dalyite.

4.1.8. Strontianite

Strontianite is a widespread accessory mineral in charoitites, and often can be observed as fine-grained mass surrounding dalyite and apatite grains (Fig. 2F, Fig. 3B and D) or presents in a form of mineral inclusions in other minerals (Fig. 3I). In some samples strontianite is xenomorphic to dalyite, suggesting latter crystallisation (Fig. 4A and B) or has close time of crystallization (Fig. 4C).

4.1.9. Tinaksite

Tinaksite is a Ti-silicate from charoitites and the main Ti-phase in charoitites, which often forms idiomorphic and hypidiomorphic crystals (Fig. 1A and B, Fig. 2M–O) up to several cm in length. Also, tinaksite can form fine-grained monomineralic aggregates. It often was observed together with dalyite (MC-112).

4.1.10. Amphibole

Amphibole (identified as potassic-magnesio-arfvedsonite) was observed in charoitites in a form of idiomorphic and hypidiomorphic crystals (Fig. 2P–R) with notable optical and chemical zoning. Its size

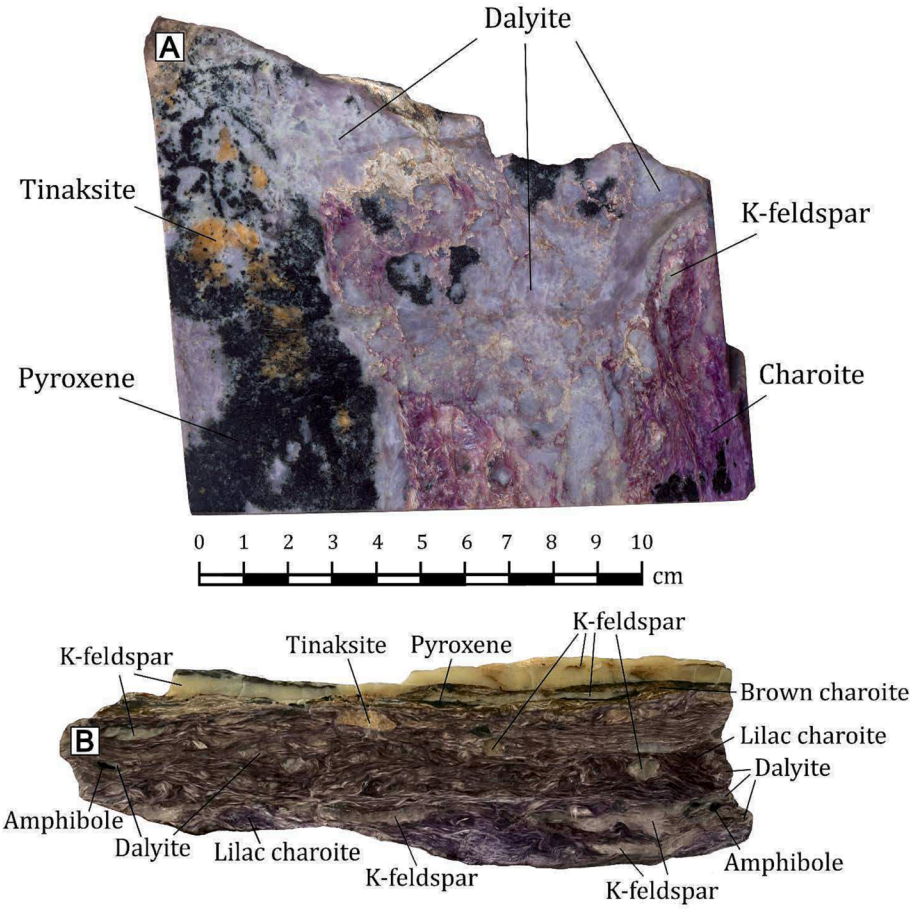

Fig. 1. Hand samples of charoite-bearing rocks with dalyite. The sample (A) belongs to Mitichkin M.A. (Vinogradov Institute of Geochemistry SB RAS). (B) Sample MC-112.

varies from 1 mm up to several cm. Dalyite was found in close intergrowth with amphibole in some samples.

4.2. Paragenetic sequence and mineral chemistry

Considering the petrographic observations, we propose the paragenetic sequence scheme (Fig. 12). According to this scheme, dalyite was formed after wadeite and close in time to tabular coarse K-feldspar (Fig. 3G).

4.2.1. Major element compositions

According to EPMA analyses (Table 1), the average compositions of dalyite from charoitites are: 62.1 ± 0.4 wt% SiO_2, 19.1 ± 1.3 wt% ZrO_2, K_2O (15.8 ± 0.2 wt%), and TiO_2 (1.7 ± 0.8 wt%). Selected major elements are plotted against SiO_2 and ZrO_2 (Fig. 6). The content of TiO_2 in dalyite from charoitites varies in different samples. In the samples MC-112 and cha-3–5 with zoned dalyite, rims of dalyite crystals are characterized by elevated TiO_2 content (Fig. 9), and cores are characterized by lower TiO_2 content and higher ZrO_2 content (Fig. 9B and C); thus, we observe increasing davanite endmember from the core towards the rim. The HfO_2 content reaches up to 0.4 wt%.

4.2.2. Trace element compositions

Dalyite from charoitites shows zircon-like chondrite-normalized REE distribution patterns (Fig. 7A) with HREE enrichment, and typical positive Ce anomaly (e.g., Hussain et al., 2020; Ngoniri et al., 2021; Rubatto, 2002). Overall REE content is relatively low with 18 ppm ∑REE on average. Compared to other silicates from charoitites (Dokuchits et al. 2022), dalyite has HREE content similar to tokkoite and coarse-grained tinaksite, but these two minerals have significantly higher LREE content than dalyite, and do not demonstrate Ce-anomaly. Charoite, frankamenite, fedorite, miserite also demonstrate LREE-enrichment, and have higher ∑REE content, than dalyite, while hydroxyapophyllite-(K) also demonstrates similar REE content (24 ppm ∑REE).

We tried to measure trace element compositions of the feather-like dalyite (Fig. 2J–R), but it was not possible to separate mineral signal from the tiny needles of charoite. Also, it was difficult to measure rim compositions with the LA–ICP–MS method in the samples cha-1–1 and MC-112, due to small sizes of crystals and abundant fluid inclusions in the grains. However, in the sample cha-3–5, which has larger crystals of dalyite (Fig. 4A and B) and no notable inclusions, the results of LA–ICP–MS, as well as EPMA, had shown Ti-Zr core-to-rim zonation. In the sample cha-3–5, cores of dalyite crystals have Ti content (ppm) from 6069 up to 9743, while in rims it varies from 10,737 up to 13380.

The Th and U contents in dalyite vary from 2 to 52 ppm (average 12 ppm) and 73 to 655 ppm (average 292 ppm), respectively. The Hf content is quite high and varies from 798 ppm (in the sample cha-1–1) to 1646 ppm (in the sample MC-112) (average 946 ppm). The average Zr/Hf ratio is 167. The Rb content is on average 418 ppm. The K/Rb ratio is, on average 325. The Rb/Sr ratio is, on average 398. The Ti/Nb is highly variable: from 139 (in the low-Ti sample cha-1–1) up to 15,010 (in the high-Ti sample MC-112).

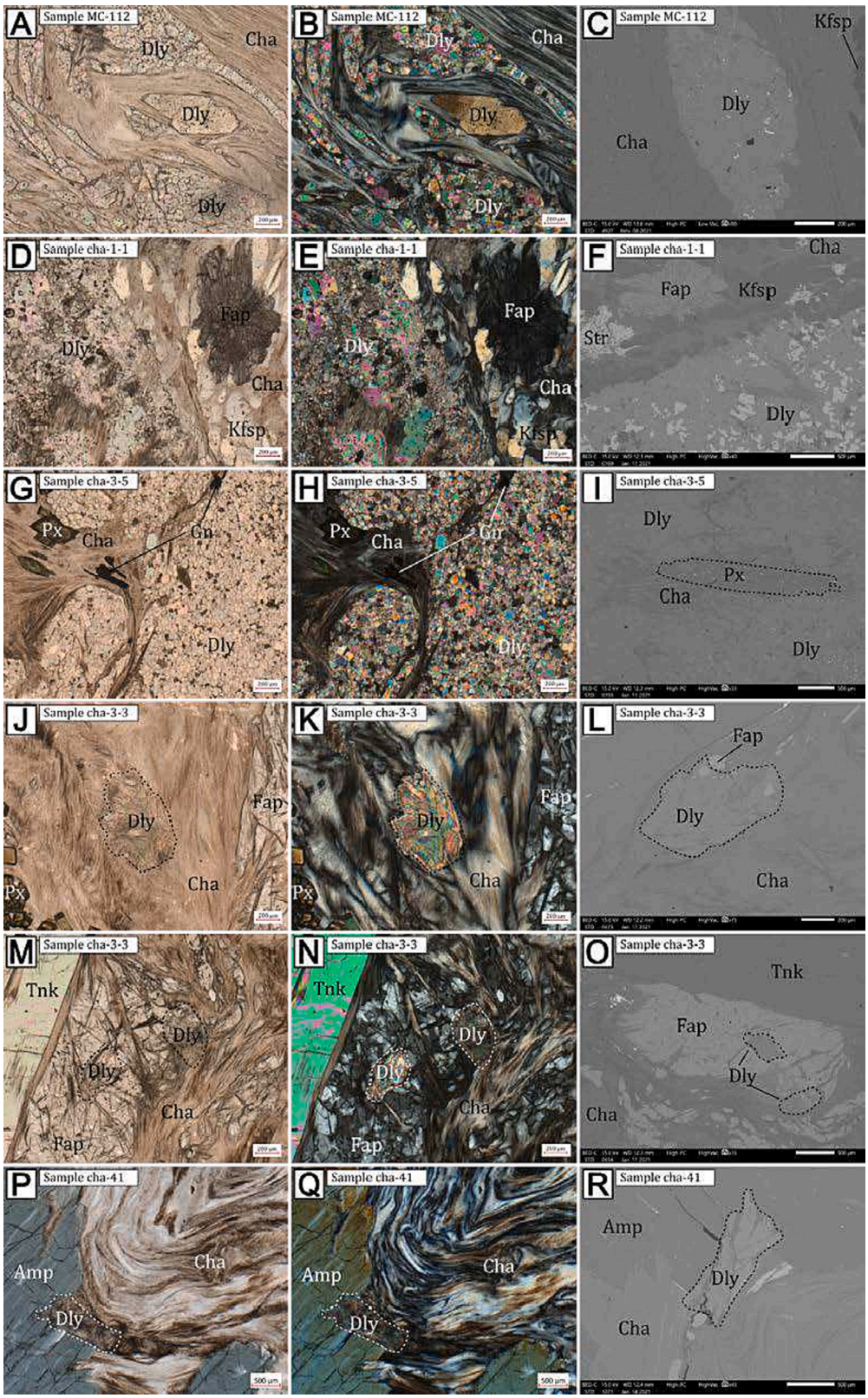

Fig. 2. Petrography of dalyite from the Sirenevyi Kamen deposit, Murun complex. A, D, G, J, M, P—parallel-polarized images; B, E, H, K, N, Q—cross-polarized images; C, F, I, L, O, R—SEM images. The minerals are: Cha—charoite; Dly—dalyite; Px—pyroxene (aegirine); Kfsp—K-feldspar (microcline); Tnk—tinaksite; Amp—alkaline amphibole (potassic-magnesio-arfvedsonite); Fap—fluorapatite; Str—strontianite; Gn—galena. Mineral symbols according to Warr (2021).

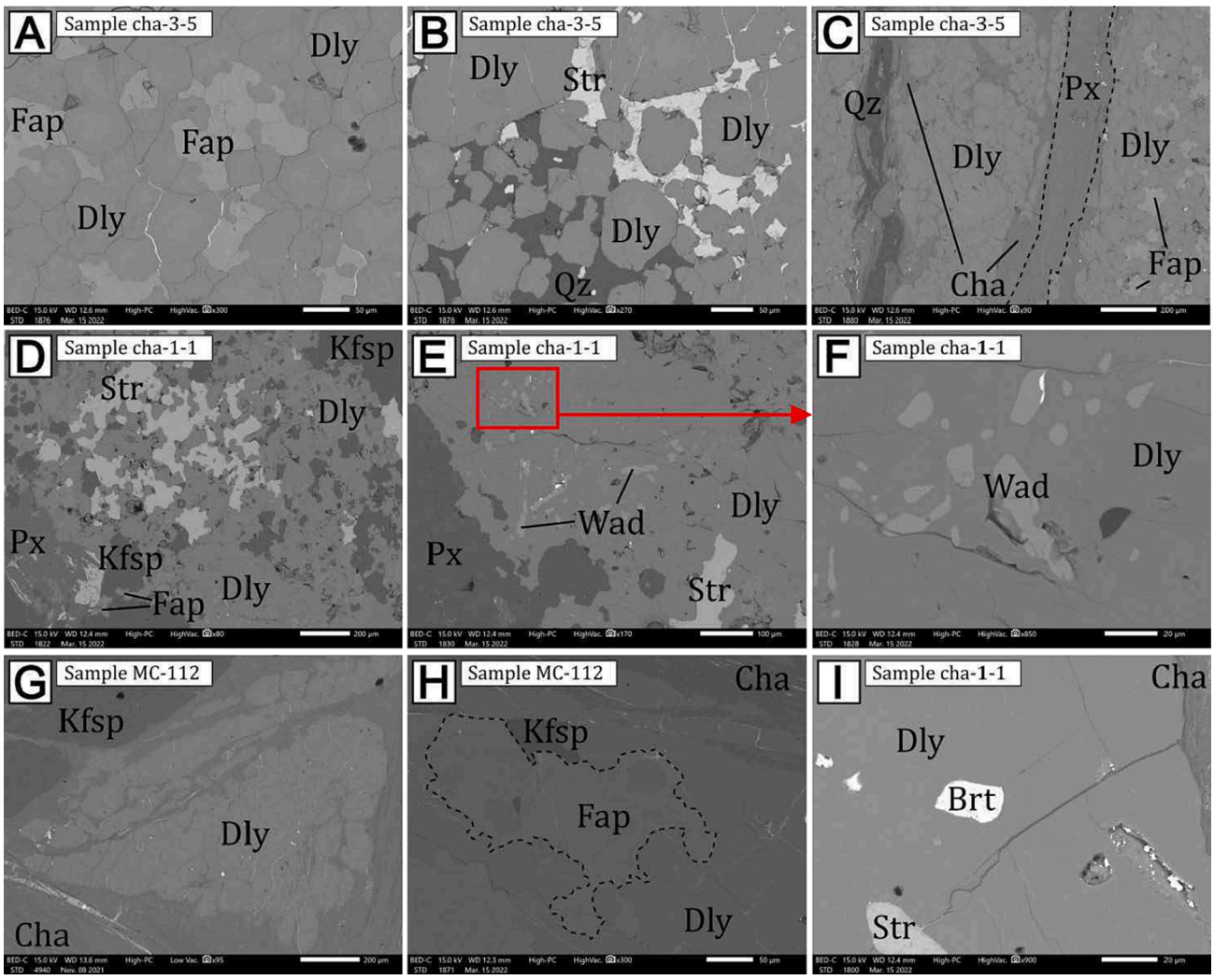

Fig. 3. Mineral associations of dalyite. The minerals are: Cha–charoite; Dly–dalyite; Px–pyroxene (aegirine); Kfsp–K-feldspar (microcline); Qz—quartz; Str—strontianite; Fap—fluorapatite; Wad—wadeite; Brt—barite.

5. Discussion

5.1. Dalyite as typical magmatic mineral of agpaitic rocks

Zirconium is a key trace element in crustal rocks used in numerous geochemical studies. In the majority of crustal rocks, the main Zr mineral is zircon [$Zr(SiO_4)$], in silica undersaturated mafic magmas this role is taken by baddeleyite [ZrO_2] and mostly by eudialyte[$Na_{15}Ca_6Fe_3Zr_3Si(Si_{25}O_{73})(O,OH,H_2O)_3(Cl,OH)_2$] in agpaitic rocks (Marks et al. 2011). Dalyite is a rare mineral with only about 20 occurrences reported in the world (Jeffery et al. 2016). The findings of dalyite are limited to magmatic rocks including peralkaline syenitic and granitic rocks, lamproites, lamprophyres and charoitites (Dolivo-Dobrovolsky and Evdokimov 1991; Jeffery et al. 2016). Dalyite and wadeite [$K_2Zr(Si_3O_9)$] appear to be the principal minerals with Zr as essential component in charoitites, while other rocks in the Murun complex (alkaline-syenitic pegmatites and pyroxene-feldspar veins) contain several Zr-silicates such as, eudialyte, and zircon (Rogova and Sidorenko 1964; Dolivo-Dobrovolsky and Evdokimov 1991; Konev et al. 1996a; Chakhmouradian and Evdokimov 1997; Reguir 2001). Temperature, pressure and activities of components are the major parameters constraining stability of a mineral. It is a question what factors could have controlled the appearance of dalyite in charoitites instead of other Zr silicates.

The occurrence of dalyite in charoitites could be discussed in the context of Zr silicate mineral associations. The petrological parameters that stabilize dalyite are high activity of K and Si, because if K activity is insufficiently then zircon crystalize and in low Si environment appears wadeite (Marks et al. 2011). Indeed, the presence of abundant quartz in charoitites proofs high Si activity and the presence of such high K minerals as charoite, tinaksite and tokkoite suggest high K activity. The inclusions of wadeite in dalyite (Fig. 3F) might indicate that wadeite crystalized in some cases first and then was replaced by dalyite as silica activity of the environment increased.

Whole rock analyses of charoitites show 200–500 ppm Zr (Vladykin 2005; Dokuchits 2016). Considering that zirconium present in other silicate minerals as trace component and average Zr content in charoite is 75 ppm, tinaksite 700–1175 ppm, tokkoite 300–460 ppm and lower Zr content in other silicates (Dokuchits et al. 2022). Therefore, dalyite is likely a main host of Zr at least in some charoitites.

The origin of charoitite is a matter of long debate with models ranging from low-temperature metasomatic (Rogova et al. 1978; Rogova 1982; Borisov 1985; Biryukov and Berdnikov 1993; Evdokimov and Reguir 1994; Konev et al. 1996a) to magmatic (Vladykin et al. 1983; Vladykin et al., 1994; Vorobiev et al. 1983). Jeffery et al. (2016) concluded that dalyite from Terceira was predominantly late-stage magmatic in origin. As a review of the occurrence of dalyite shows that the mineral is characteristic for magmatic rocks (Jeffery et al. 2016), it could be argued that the occurrence of dalyite in charotites is

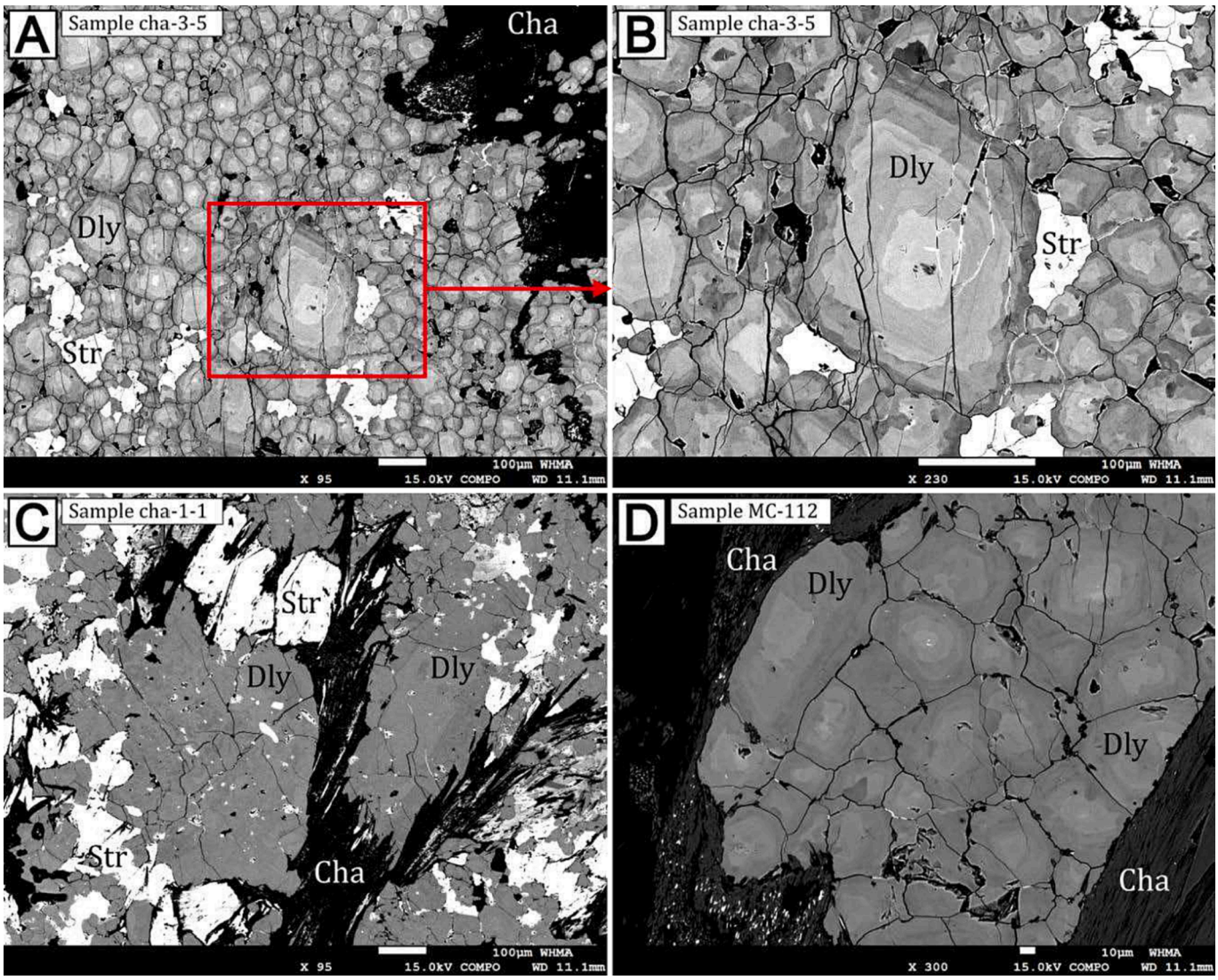

Fig. 4. Backscattered electron images of dalyite aggregates, showing notable chemical zoning. The minerals are: Dly—dalyite, Cha—charoite, Str—strontianite.

an evidence for formation of these rocks by magmatic processes as proposed by Vladykin (2005) and Vladykin et al. (2018).

5.2. Constraints of stability of dalyite

Experimental constraints on pressure stability of dalyite are not available yet, however some inference could be made from the occurrences and properties of the mineral. The findings of dalyite could be divided to volcanic rocks such as granite ejecta (Ascension island) (Van Tassel and Hey, 1952) and syenite ejecta (Agua de Pau) Iwagi Islet, Japan (Imaoka et al. 2021); hypabyssal intrusions such as Sunnfjord and lamproites of Cancarix complex, Spain (Linthout et al. 1988); and rocks in large plutonic complexes such as Lovozero complex (Ivanyuk et al. 2006). The Murun complex is composed of several laccolites that intruded in shallow depth (Vorobiev 2008). The geology and occurrence of effusive rocks in the Murun complex indicates that charoitites have formed in near surface conditions (Vorobiev 2008). Studies of fluid inclusions estimated pressure of 0.6–4 kbar in charoitites, 2.4–5.5 kbar in carbonatites, and <1.2 kbar in torgolites (Prokofiev and Vorobiev 1991), confirming that charoitites formed at low pressure.

The structure of dalyite characterized by crystal structure with large channels and pores (Fleet 1965). Dalyite has relatively low density of 2.82 g/cm^3 that is much lower than density of other zirconium silicates such as zircon (4.65 g/cm^3), baddeleyite (5.75 g/cm^3) and zirconolite (4.38 g/cm^3). The phases of low density typically favored at low pressure, and at higher pressure stabilize mineral with higher density (Gibbs 1906). Therefore, the occurrence of dalyite in the low-pressure rocks and the properties of the mineral might indicate that it is characteristic for low pressure environment, however this hypothesis should be tested experimentally.

5.3. On the potential of geothermometry from Ti in dalyite

Titanium could be a particularly important impurity in Zr silicate minerals. The similarity of the ionic radius of Ti^{4+}(0.74 Å) to Zr^{4+}(0.84 Å) results in limited mutual solid solutions between Zr and Ti minerals that are sensitive to temperature and can be used as geothermometers. The examples include Ti in zircon (Watson et al. 2006), Ti in quartz (Wark and Watson 2006), Zr in rutile (Zack et al. 2004), and Zr in titanite (Hayden et al. 2008). Titanium impurity in dalyite could be investigated as a potential geothermometer, which might bring additional information on temperatures of formation of charoitites and other agpaitic rocks.

Dalyite from Japan (Imaoka et al. 2021), Portugal (Jeffery et al. 2016), Spain (Linthout et al. 1988), and Norway (Furnes et al. 1982; Robins et al. 1983) have low concentrations of TiO_2 (0.1–1.2 wt%). In

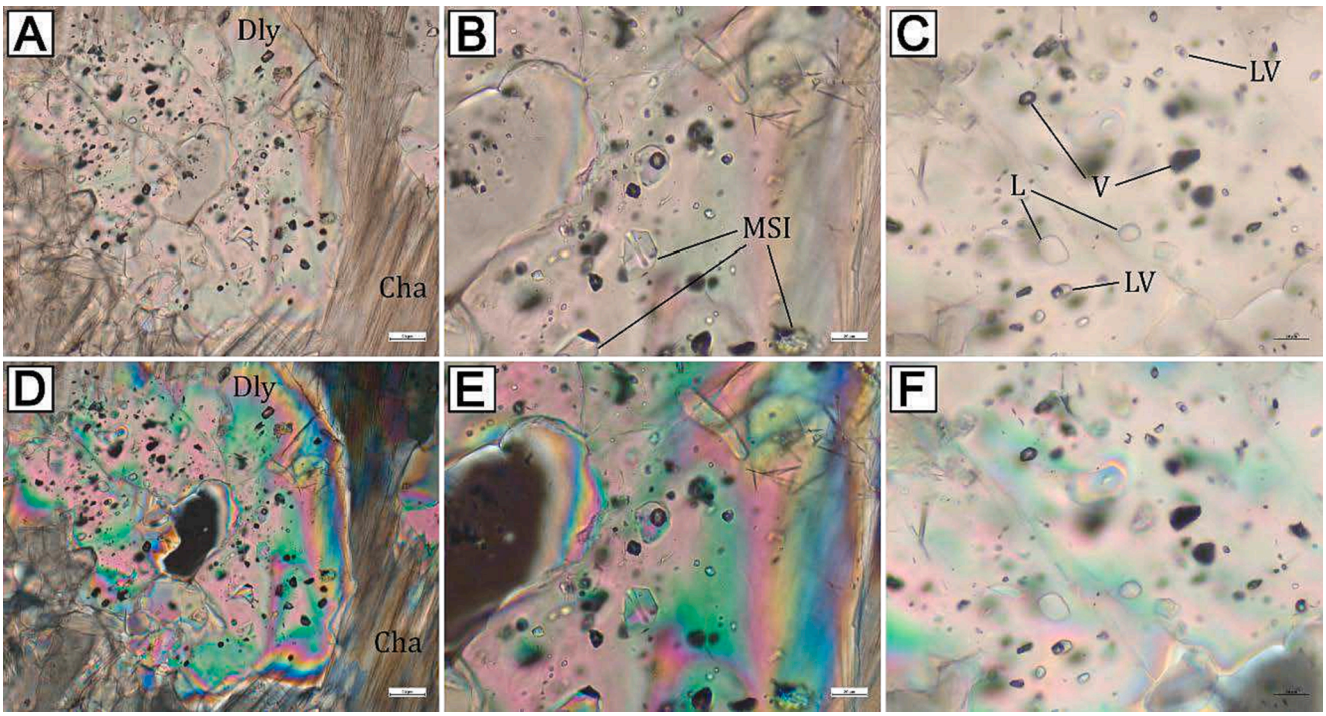

Fig. 5. Abundant inclusions in dalyite. A, B, C—parallel-polarized images; D, E, F—cross-polarized images. Dly—dalyite; Cha—charoite; MSI—multiphase solid inclusions; LV—liquid–vapor fluid inclusions; L—liquid-type fluid inclusions; V—vapor-type fluid inclusions.

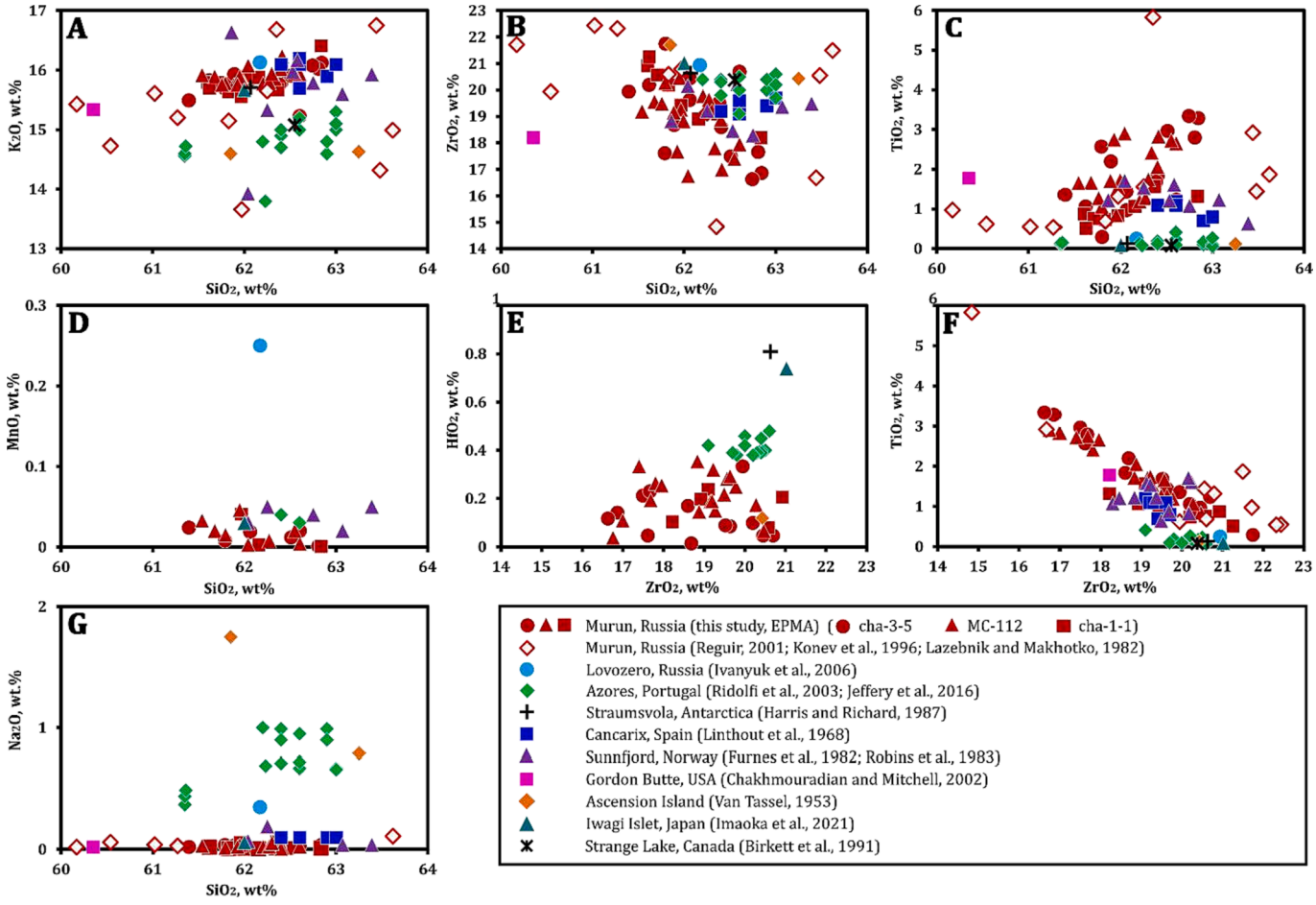

Fig. 6. Binary diagrams of major elements of dalyite from different localities. The data sources are shown in the captions. Data for Na, Hf, Mn and Ti is presented where analyses permit.

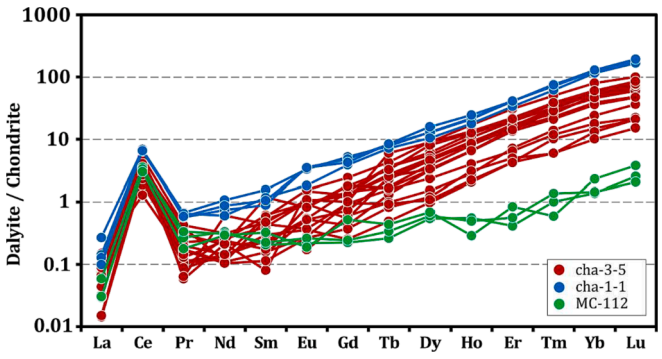

Fig. 7. Chondrite normalized REE patterns of Murun dalyite (this study). Chondrite composition is according to McDonough and Sun (1995).

our analyses Ti content varies from 0.1 to 3.3 wt% TiO_2, in agreement with data of Konev et al. (1996b) who reported TiO_2 content reaching 5.9 wt% in Murun dalyite (Fig. 6C, F). Lazebnik and Makhotko (1982) analyzed dalyite from fenite, carbonatite, charoitite, and aegirinite from the Murun complex and reported <1 wt%. TiO_2 in dalyite from carbonatites. The average Ti concentration in dalyite from charoitites can be compared to tokkoite (Lazebnik et al. 1986; Lacalamita et al. 2017), which also contains about 2 wt% of TiO_2.

Jeffery et al. (2016) modelled energy of different substitution mechanisms of Ti in dalyite and considered Ti in positions of K, Zr and Si. The substitution of Ti to K position was highly unfavorable. Both Si and Zr positions were concluded possible from the calculations. The negative correlation of Zr and Ti in dalyite (Fig. 6F) and the absence of correlation of Si vs Ti (Fig. 6C) suggest that Ti substitutes Zr in Murun dalyite. The study of Zr^{4+}-Ti^{4+} solid solution by Konev et al. (1996a) had shown that in titaniferous dalyite, davanite endmember can reach

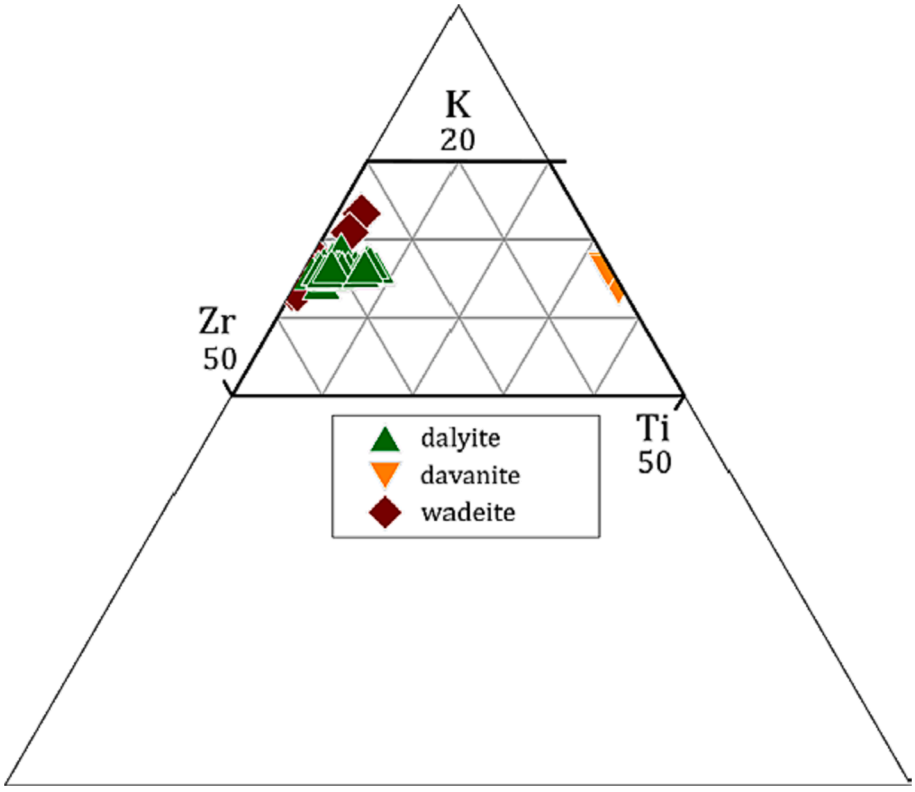

Fig. 8. Ternary diagram of molar content of K, Zr, and Ti in dalyite and davanite from the rocks of Murun complex. Dalyite composition: this study; davanite composition from Lazebnik et al. (1984); wadeite composition from (Rogova and Sidorenko 1964; Mitchell and Vladykin 1993; Konev et al. 1996a; Reguir 2001).

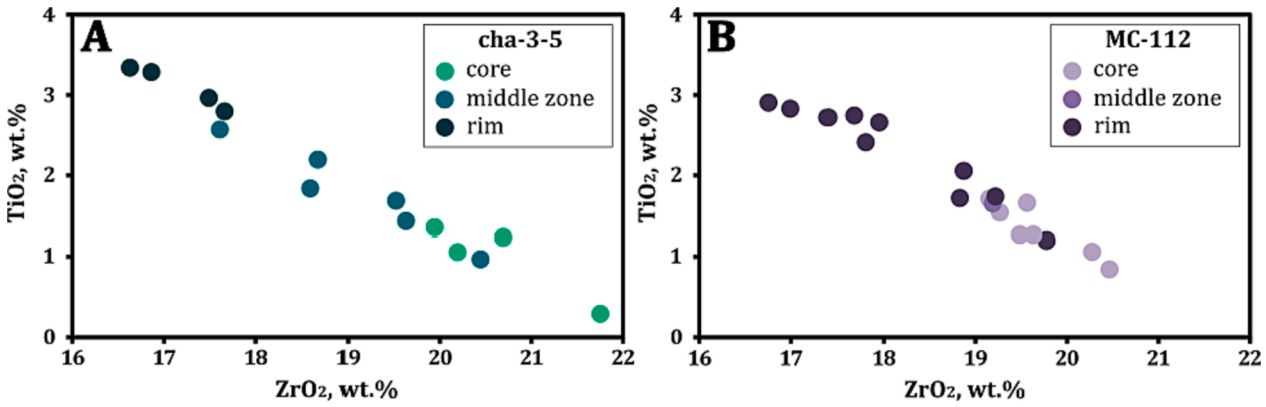

Fig. 9. Zr-Ti binary diagrams of zoned dalyite (this study).

20–40 wt%. Titanium has been proposed to be a part of the mineral formula of dalyite in Konev et al. (1996b) as $K_2(Zr_{0.6}Ti_{0.4})Si_6O_{15}$. In our analyses Zr^{4+} varies from 0.8 up to 1.0 apfu (Fig. 10A), and Ti^{4+} varies from 0.02 (in cores) up to 0.2 apfu (in rims). Considering the variability of dalyite composition the formula of the mineral could be presented as $K_2(Zr_{1-x}Ti_x)Si_6O_{15}$. The plot of dalyite from charoitites and davanite from quartz-K-fsp-calcite rocks of Murun complex, from our and previously published data on a ternary Zr–Ti–K diagram shows that the compositions lie close to theoretical substitution line between dalyite and davanite (Fig. 8).

The example of Ti in zircon geothermometer (Watson et al. 2006) shows that the content of a component is defined by temperature as well as activity of the components in the system. The crystals of dalyite from sample cha-3–5 show systematic zonation with the increase of Ti content from the cores to rims (Fig. 9; Table 1). The normal evolution of a system is one with the continuous decrease of temperature and it is reasonable to suggest that the cores formed earlier and at higher temperature than the rims. The fact that Ti content increases allows to speculate that Ti activity was more important factor than temperature controlling Ti content in dalyite.

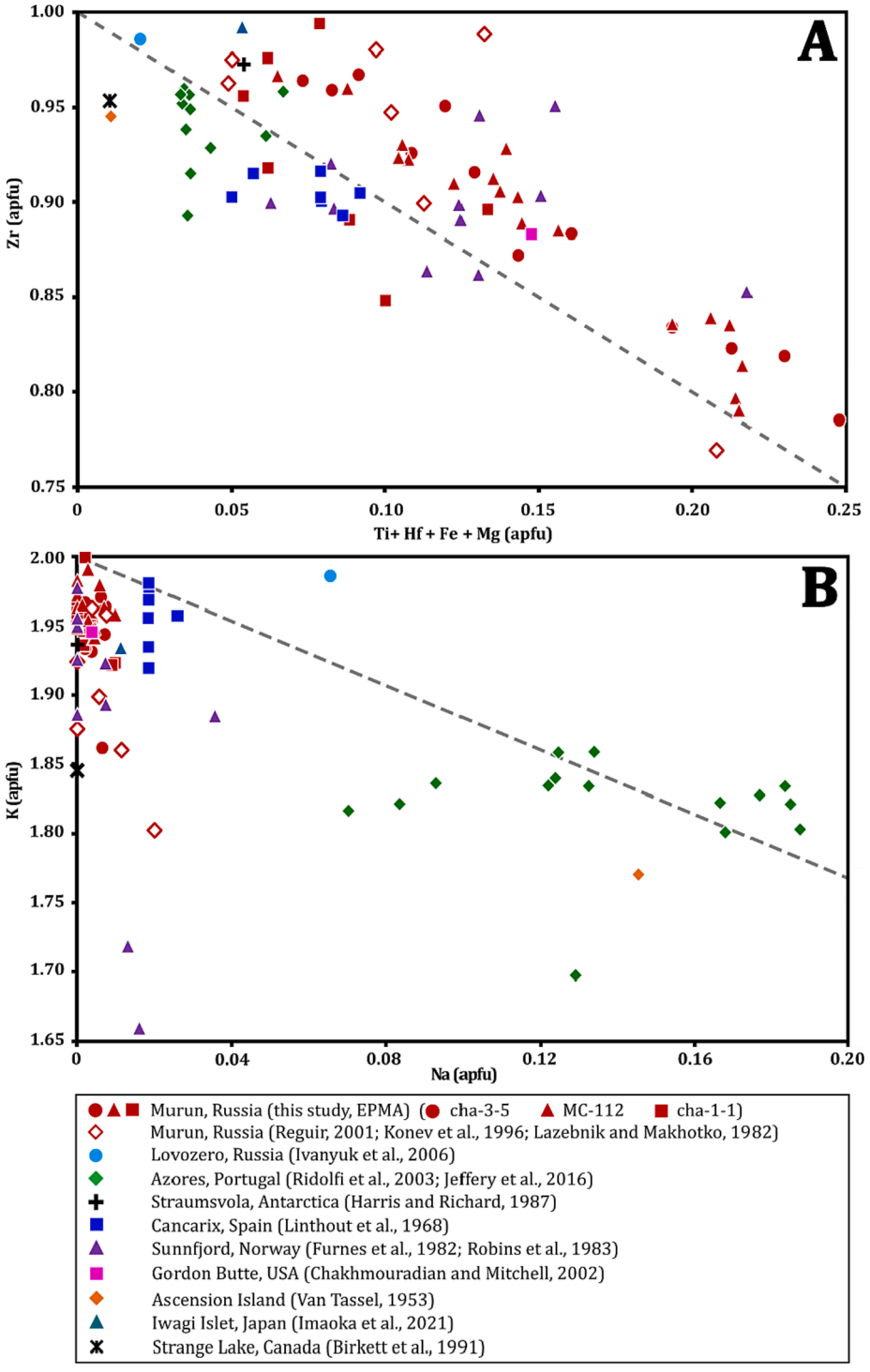

Fig. 10. Zr versus (Ti + Hf + Fe + Mg), apfu (A), and K versus Na, apfu (B) diagrams of dalyite from different locations.

Murun complex has rich association of Ti-minerals: tinaksite [$K_2Na(Ca,Mn^{2+})_2TiO[Si_7O_{18}(OH)]$] (up to 11 wt% TiO_2), titanite [$CaTi(SiO_4)O$] (up to 39 wt% TiO_2), davanite [$K_2TiSi_6O_{15}$] (up to 15 wt% TiO_2), yuksporite [$K_4(Ca,Na)_{14}(Sr,Ba)_2(\square,Mn,Fe)(Ti,Nb)_4(O,OH)_4(Si_6O_{17})_2(Si_2O_7)_3(H_2O,OH)_3$] (up to 11 wt% TiO_2), narsarsukite [$Na_4(Ti,Fe)_2[Si_8O_{20}](O,OH,F)_2$] (up to 16 wt% TiO_2), ilmenite [$Fe^{2+}TiO_3$] (up to 60 wt% TiO_2), titaniferous magnetite [$Fe^{2+}(Fe^{3+},Ti)_2O_4$] (up to 4 wt% TiO_2), and others, which were found in different rocks of the complex, including the area of the Sirenevyi Kamen deposit (Rogov et al. 1965; Lazebnik et al. 1984; Lazebnik et al. 1985; Lazebnik et al. 1986; Konev et al. 1985; Konev et al., 1996a; Chakhmouradian and Evdokimov 1997; Mesto et al. 2015; Lacalamita et al. 2017; Schingaro et al. 2017). Significant quantities of TiO_2 in early rock-forming minerals of charoitites, such as tinaksite (up to 10 wt%) (Rogov et al. 1965; Vladykin et al. 1983; Reguir 2001; Kaneva 2014; Wang et al. 2014; Dokuchits et al. 2022) and pyroxene (up to 2.3 wt%) (Vladykin et al. 1983; Reguir 2001; Wang et al. 2014), are an evidence of presence of Ti in the system during crystallization of dalyite. However, which mineral controlled Ti activity in charoitites need to be clarified in the future studies.

Overall, Ti content in dalyite shows systematic variations between samples and rock types. It is possible that Ti content in dalyite has a significant temperature dependence and experimental studies of dalyite stability and composition are desirable. However, Ti content in dalyite is likely to be sensitive to the activity of Ti and considering that Ti in charoitites is hosted by complex minerals such as tinaksite, this parameter could be difficult to estimate in charoitites limiting the utility of such a geothermomether.

5.4. Lattice environment of impurities in dalyite

Sodium is one of the major components in dalyite from some localities and could have genetic implications (Jeffery et al. 2016). The Na_2O content does not exceed 0.6 wt% in dalyite from all the localities (Fig. 6G), except for those from Ascension Island (granite) (Van Tassel 1952), which contains up to 1.8 wt% Na_2O. In dalyite from Murun complex, Na content is reported to be very low or below detection limit in Konev et al. (1996b) (EPMA; bdl); Lazebnik and Makhotko (1982) (EPMA; bdl in charoitites, up to 0.11 wt% in fenite); Reguir (2001) (SEM, bdl), and in this study as well (EPMA and LA–ICP–MS; bdl up to 0.05 wt%). Jeffery et al. (2016) subdivided dalyite from Terceira (syenitic ejecta) to two groups with different Na content. The variations in Na content led to discussion of the role of metasomatic processes and crystallization from small volume residual melt. In this study, Na has been measured both by EPMA and LA–ICP–MS. LA–ICP–MS obtained slightly lower limits of detection (about av. 90 ppm vs av. 120 ppm by EPMA). The high content of Na in minerals of charoitites, which crystallized before and after dalyite (Fig. 12), including charoite and aegirine indicates that Na was abundantly available during crystallization of dalyite. This raises a question of what factors that control Na content in dalyite.

Sodium likely occupies K position in dalyite structure (Fleet 1965). Solid solutions between Na and K are common in nature with the most important example being alkali feldspar. The extent of solid solutions between Na and K in silicate minerals of charoitites has been summarized by Dokuchits et al. (2022), and demonstrated that in most minerals the range of Na–K solid solution was limited. This was attributed to relatively low temperature of crystallization and high volatiles content of the mineral-forming media that resulted in low solubility between Na and K. The same factors likely acted in the case of dalyite crystallization.

REE could act as a probe of the crystallochemical environment in the mineral structure and reveal the surrounding of REE in dalyite structure. The REE patterns of dalyite show a number of characteristic features such as HREE enrichment, steep decrease of LREE and positive Ce anomalies (Fig. 7) typical for magmatic and metamorphic zircon (e.g. Stepanov et al. 2016). Positive Ce anomaly is an extremely rare feature in minerals and is truly common only for zircon and some rare minerals of Ce^{4+} (Zhukova et al. 2021).

Little is known so far about the structural position of REE in dalyite. The crystal structure of dalyite composed of sheets of four-, six- and eight-membered rings of SiO_4 tetrahedra. These sheets are linked by ZrO_6 octahedra and irregular KO_8 polyhedra (Fleet 1965). The average Zr-O distance is 2.06 A (±0.03 A) (Fleet 1965), which is slightly lower than the Zr-O distance of 2.13–2.27A in zircon structure (Finch and Hanchar 2003). The similarity of REE patterns to zircon indicate that surrounding of REE in dalyite structure is similar to Zr in zircon and REE reside in Zr position. Similar to other silicates of charoitites, the REE patterns of dalyite do not display any evidence of Eu anomaly (Fig. 7). This feature is evidence of absence of plagioclase fractionation during crystallization of the rocks (Dokuchits et al. 2022).

Uranium is a common trace element in Zr-minerals. In the three samples it varies significantly; the dalyite from sample cha-1–1 has on average 340 ppm U, while MC-112 dalyite has on average only 74 ppm U. The Th/U ratio is quite low in all the grains, and is, on average 0.05. The preference of dalyite to U relative to Th is another manifestation of the similarity of partitioning to Zr position to zircon that is known for preference to HREE and U (Rubatto and Hermann 2007).

Hafnium is a principal impurity in Zr-bearing minerals. The reason lies in the fact that both Zr and Hf present in the same group of the periodic table, have identical structure of the outer shell, as well as close ionic radiuses: 0.72 Å for Zr^{4+}, and 0.71 Å for Hf^{4+}, and have identical chemistry. Dalyite from charoitites contains up to 0.3 wt% HfO_2, which is close to dalyite from Azores, Portugal (0.4 wt% HfO_2), reported by Jeffery et al. (2016) (Fig. 6E). Dalyite from Japan (Imaoka et al. 2021) has elevated HfO_2, reaching 0.7 wt%. The Zr/Hf ratio of dalyite from charoitites reaches 167 on average (Fig. 11), and in zoned sample cha-3–5, it varies from 146 (in the rim) up to 195 (in the core), that is significantly higher than chondritic ratio of 34.2 (e.g. Ewing et al., 2014). Hafnium content in zoned sample cha-3–5 varies from 811 ppm (in the core) up to 948 (in the rim). This indicates that either formation of charoitites has been associated crystallization of minerals with strong preference to Hf, or dalyite preference to Zr. The variability of Zr/Hf of dalyite indicates that Hf could be a sensitive indicator of the mineral origin.

6. Conclusions

Dalyite is an important Zr-silicate mineral of peralkaline agpaitic rocks. It is typically of magmatic origin, and likely forms at low-pressure conditions. Composition of dalyite such as content of Ti, Na, Hf and trace elements is sensitive to the conditions and mechanism of mineral formation. In Murun charoitites REE patterns resemble patterns typical for zircon and suggest similar crystallochemical environment of REE in mineral structure. Dalyite has elevated content of Nb (10 ppm) and Ta (1 ppm). These concentrations are lower than Nb and Ta in tinaksite and tokkoite, and comparable to Nb and Ta content in other rare Ca-silicates of charoitites such as charoite. The elevated content of Nb and Ta in dalyite could be explained by the affinity of Nb and Ta to Ti that is evident from the commonly enrichment of Ti-bearing minerals. Dalyite from charoitites is generally defined by Ti ↔ Zr substitution with the increasing of davanite endmember from the cores toward the rims.

Chemical zoning, reaction rims and inclusions in minerals can be useful for recovery of complex histories (such as fractionation, multistage activities of fluids etc.). In charoitites, several minerals demonstrate chemical zonation (pyroxene, amphibole, strontian fluorapatite, steacyite and dalyite). Future studies on stability and trace element composition of dalyite will allow better understanding of crystallization conditions of rare agpaitic rocks.

Declaration of Competing Interest

The authors declare that they have no known competing financial interests or personal relationships that could have appeared to influence

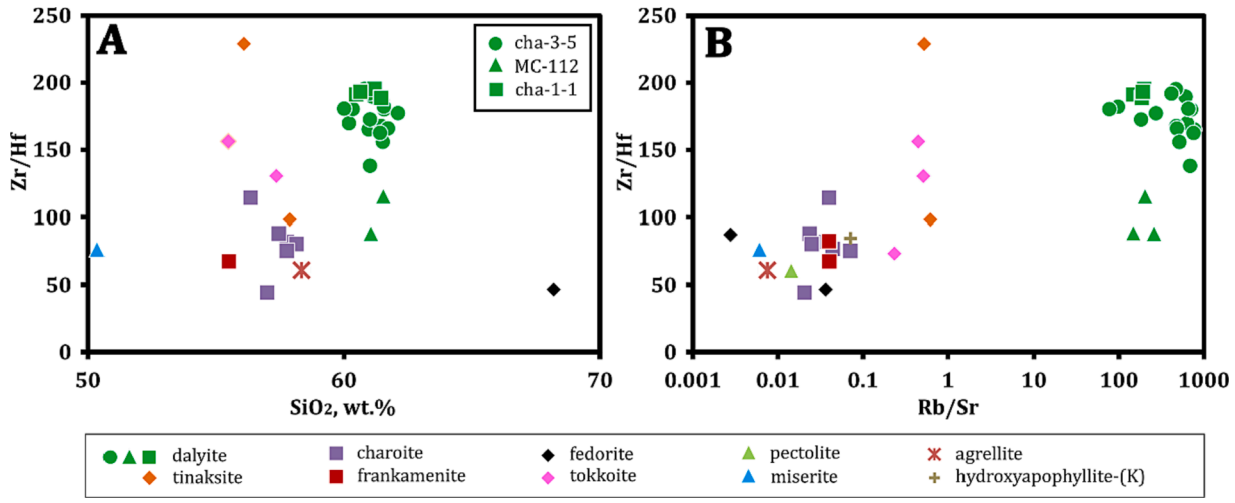

Fig. 11. Zr/Hf versus SiO_2 (wt.%) (A) and Z/Hf versus Rb/Sr (B). Dalyite: this study; other minerals: Dokuchits et al. (2022).

Mineral	Paragenetic Sequences		
	Early stage	Middle stage	Late stage
Aegirine	I		II
Strontian fluorapatite			
Tinaksite			
Amphibole			
K-feldspar	I		II
Wadeite			
Dalyite			
Steacyite			
Quartz			
Sulfides			
Barite			
Strontianite			
Charoite			

Fig. 12. Paragenetic sequence in charoitites including dalyite.

the work reported in this paper.

Data availability

All data are included in the paper

Acknowledgments

The authors thank Sheng-Bin Guo for assistance with EPMA measurement of dalyite from charoitites. Mitichkin M.A. from Vinogradov Institute of Geochemistry SB RAS is thanked because he provided us a beautiful sample of charoitite with dalyite from the Figure 1. This study was supported by the National Natural Science Foundation of China Project (No. 42050410318) and the Special Fund from the State Key Laboratory of Geological Processes and Mineral Resources, China University of Geosciences (No. MSFGPMR03-2).

References

Aja, S.U., Wood, S.A., Williams-Jones, A.E., 1996. The solubility of some alkali-bearing Zr minerals in hydrothermal solutions. MRS Online Proceeding Library Archive 432, 69–74.

Biryukov, V.M., Berdnikov, N.V., 1993. The paragenetic relation between charoite mineralization and alkali metasomatism. International Geology Review 35 (7), 585–602.

Borisov, A.B., 1985. To the time and conditions for the formation of charoite rocks of different textures. Zapiski Vsesoyuznogo Mineralogicheskogo Obshchestva 113, 455–463. In Russian.

Borisov, B.A., Evdokimov, M.D., 1984. Fenites of the charoite occurrence area of the Murun complex. Zapiski Vsesoyuznogo Mineralogicheskogo Obshchestva 4, 485–497. In Russian.

Cann, J.R., 1967. A second occurrence of dalyite and the petrology of some ejected syenite blocks from São Miguel, Azores. Mineralogical Magazine 36 (278), 227–232.

Chakhmouradian, A.R., Evdokimov, M.D., 1997. Zirconium and titanium mineralization in alkaline-syenitic pegmatites of Malomurunsky massif, Yakutiya. Zapiski Vserossijskogo Mineralogicheskogo Obshchestva 126, 32–42. In Russian.

Chakhmouradian, A.R., Cooper, M.A., Ball, N., Reguir, E.P., Medici, L., Abdu, Y.A., Antonov, A.A., 2014. Vladykinite, Na3Sr4(Fe2+Fe3+)Si8O24: A new complex sheet silicate from peralkaline rocks of the Murun complex, eastern Siberia, Russia. American Mineralogist 99, 235–241.

Dokuchits, E.Y., 2016. Mineralogical and geochemical features of rocks of the charoitic deposit, Murun complex. Vinogradov Institute of geochemistry SB RAS, Irkutsk, Russia (In Russian). PhD Thesis.

Dokuchits, E.Y., Jiang, S.-Y., Stepanov, A.S., Zhukova, I.A., Radomskaya, T.A., Marfin, A. E., Vishnevskiy, A.V., 2022. Geochemistry of Ca-(K)-(Na) silicates from charoitites in the Sirenevyi Kamen gemstone deposit, Murun Complex, Eastern Siberia. Ore Geology Reviews 143, 104787.

Dolivo-Dobrovolsky, D.V., Evdokimov, M.D., 1991. Zirconium mineralization of alkaline metasomatites of the Murun complex. Zapiski Vsesoyuznogo Mineralogicheskogo Obshchestva 1, 99–105. In Russian.

Evdokimov, M.D., Reguir, E.P., 1994. Canasite in charoitites from the Murun alkaline complex. Zapiski Vserossijskogo Mineralogicheskogo Obshchestva 123, 104–118. In Russian.

Ewing, T., Rubatto, D., Hermann, J., 2014. Hafnium isotopes and Zr/Hf of rutile and zircon from lower crustal metapelites (Ivrea–Verbano Zone, Italy): Implications for chemical differentiation of the crust. Earth and Planetary Sciences Letters 389, 106–118.

Finch, R.J., Hanchar, J.M., 2003. Structure and Chemistry of Zircon and Zircon-Group Minerals. Reviews in Mineralogy and Geochemistry 53 (1), 1–25.

Fleet, S.G., 1965. The crystal structure of Dalyite. Zeitschrift fur Kristallographie 121 (5), 349–368.

Furnes, H., Mitchell, J.G., Robins, B., Ryan, P.D., Skjerlie, F.J., 1982. Petrography and geochemistry of peralkaline, ultrapotassic syenite dykes of Middle Permian age, Sunnfjord, West Norway. Norsk Geologisk Tidsskrift 3, 147–159.

Gibbs, J.W., 1906. The Scientific Papers of J. Willard Gibbs, Vol. I: Thermodynamics, 434 p. Vol. I. Unabridged and unaltered Dover Publications reprint of 1906 edition, New York.

Hayden, L.A., Watson, E.B., Wark, D.A., 2008. A thermobarometer for sphene (titanite). Contributions to Mineralogy and Petrology 155 (4), 529–540.

Hussain, A., Zhao, K.-D., Arif, M., Palmer, M.R., Chen, W., Zhang, Q., Li, Q., Jiang, S.-Y., Girei, M.B., 2020. Geochronology, mineral chemistry and genesis of REE mineralization in alkaline rocks from the Kohistan Island Arc, Pakistan. Ore Geology Reviews 126, 1–24.

Imaoka, T., Akita, S., Nagashima, M., 2021. Dalyite ($K_2ZrSi_6O_{15}$) and Zektzerite ($LiNaZrSi_6O_{15}$) in Aegirine-bearing Albitite from Iwagi Islet, SW Japan. Journal of Geography (Chigaku Zasshi) 130, 369–378.

Ivanov, A.V., Vladykin, N.V., Demonterova, E.I., Gorovoy, V.A., Dokuchits, E.Y., 2018a. $^{40}Ar/^{39}Ar$ geochronology of the Malyy (Little) Murun Massif, Aldan Shield of the Siberian Craton: A simple story for an intricate igneous complex. Minerals 602, 1–21.

Ivanov, A.V., Gorovoy, V.A., Gladkochub, D.P., Shevelev, A.S., Vladykin, N.V., 2018b. The first pPrecise data on the age of charoite mineralization (Eastern Siberia, Russia). Doklady Earth Sciences 478, 179–182.

Ivanyuk, G.Y., Pakhomovsky, Y.A., Yakovenchuk, V.N., Menshikov, Y.P., Bogdanova, A. N., Mikhailova, Y.A., 2006. Rare-metal minerals of microcline-quartz veins in volcanogenic-sedimentary rocks of Kitknyun Mt (Lovozero massif). Zapiski Vserossijskogo Mineralogicheskogo Obshchestva, CXXXV 66–81. In Russian.

Jeffery, A.J., Gertisser, R., Jackson, R.A., O'Driscoll, B., Kronz, A., 2016. On the compositional variability of dalyite, K2ZrSi6O15: a new occurrence from Terceira, Azores. Mineralogical Magazine 80 (4), 547–565.

Kaneva, E.V., 2014. Crystal Structure and crystal chemical studies of minerals of alkaline rocks from Russia, Tajikistan and Mongolia. Universita'DegliStudi Di Bari "Aldo Moro", Italy. PhD Thesis,.

Kaneva, E.V., Radomskaya, T.A., Suvorova, L., Sterkhova, I., Mitichkin, M.A., 2020. Crystal chemistry of fluorcarletonite, a new mineral from the Murun alkaline complex (Russia). European Journal of Mineralogy 32, 137–146.

Konev, A.A., Vorobiev, E.I., and Lazebnik, K.A., 1996a. Mineralogy of the Murunsky Alkaline Massif, Publishing House of SB RAS., 221 p. Sci. Res. Center Trofimuk Inst. Petrol. Geol. Geophys., Siberian Branch Russ. Acad. Sci., Novosibirsk (In Russian).

Konev, A.A., Vorobiev, E.I., Sapozhnikov, A.N., Malyshonok, Y.V., Paradina, L.F., Lapides, I.L., 1985. New data on yuksporite. Mineralogical Journal 7, 74–78.

Konev, A.A., Rastsvetaeva, R.K., Evsunin, V.G., Kashaev, A.A., Uschapovskaya, Z.F., 1996b. Titaniferous dalyite from the Murun massif. Zapiski Vserossijskogo Mineralogicheskogo Obshchestva 1, 81–88. In Russian.

Lacalamita, M., Mesto, E., Kaneva, E., Scordari, F., Pedrazzi, G., Vladykin, N., Schingaro, E., 2017. Structure refinement and crystal chemistry of tokkoite and tinaksite from the Murun massif (Russia). Mineralogical Magazine 81 (2), 251–272.

Lazebnik, K.A., Lazebnik, Y.D., 1981. Rare silicates, miserite, canasite and fedorite in charoitic rocks. Mineralogy and Geochemistry of Ultramafic and Mafic Rocks of Yakutia 32–50. In Russian.

Lazebnik, K.A., Lazebnik, Y.D., 1983. Mineralogy of K-fenites, Inarigda River (South Yakutiya). Silicates of magmatic and postmagmatic formations of Yakutiya 20–27. In Russian.

Lazebnik, K.A., Lazebnik, Y.D., Makhotko, V.F., 1984. Davanite - a new alkaline Ti-silicate (K2TiSi7O15). Zapiski Vsesoyuznogo Mineralogicheskogo Obshchestva 113, 81–84. In Russian.

Lazebnik, K.A., Makhotko, V.F., 1982. Dalyite - the first found in the USSR. Zapiski Vsesoyuznogo Mineralogicheskogo Obshchestva 111, 287–293. In Russian.

Lazebnik, K.A., Makhotko, V.F., Lazebnik, Y.D., 1985. First discovery of priderite in Eastern Siberia. Mineralogical Journal 7, 81–83. In Russian.

Lazebnik, K.A., Nikishova, L.V., Lazebnik, Y.D., 1986. Tokkoite a new mineral of charoitites. Mineralogical Journal 8, 81–83. In Russian.

Linthout, K., Nobel, F.A., Lustenhouwer, W.J., 1988. First occurrence of dalyite in extrusive rock. Mineralogical Magazine 52 (368), 705–708.

Liu, Y., Hu, Z., Gao, S., Günther, D., Xu, J., Gao, C., Chen, H., 2008. In situ analysis of major and trace elements of anhydrous minerals by LA-ICP-MS without applying an internal standard. Chemical Geology 257 (1-2), 34–43.

Marks, M.A.W., Hettmann, K., Schilling, J., Frost, B.R., Markl, G., 2011. The mineralogical diversity of alkaline igneous rocks: critical factors for the transition from miaskitic to agpaitic phase assemblages. Journal of Petrology 52 (3), 439–455.

McDonough, W.F., Sun, S.-s., 1995. The composition of the Earth. Chemical Geology 120 (3-4), 223–253.

Mesto, E., Kaneva, E.V., Lacalamita, M., Schingaro, E., Scordari, F., and Vladykin, N.V., 2015. Structural disorder in Narsarsukite from Murun (Russia). In An International Journal of Mineralogy, Crystallography, Geochemistry, Ore deposits, Petrology, Volcanology and applied topics on Environment, Archaeometry and Cultural Heritage pp. 123–124.

Mitchell, R.H., Vladykin, N.V., 1993. Rare-earth element-bearing tausonite and potassium barium titanites from the Little Murun potassic alkaline complex, Yakutia, Russia. Mineralogical Magazine 57, 651–664.

Mitchell, R.H., Smith, C.B., Vladykin, N.V., 1994. Isotopic composition of strontium and neodymium in potassic rocks of the Little Murun complex, Aldan Shield, Siberia. Lithos 32 (3-4), 243–248.

Ngoniri, A.H., Djomo, H.D., Ngnotue, T., Kenne, P.A., Mbianya, G.N., Ganno, S., Nzenti, J.P., 2021. Zircon Trace Element Geochemistry and Ti-in-Zircon Thermometry of the Ngazi-Tina Pan-African Post-Collisional Granitoids, Adamawa Cameroon. International Journal of Geosciences 12 (04), 307–328.

Nikishova, L.V., Lazebnik, K.A., Rozhdestvenskaya, I.V., Emel'yanova, N.N., Lazebnik, Y. D., 1996. Frankamenite $K_2Na_3Ca_5(Si_{12}O_{30})F_3(OH)H_2O$ - a new mineral, triclinic variety of canasite from charoitites. Zapiski Vserossijskogo Mineralogicheskogo Obshchestva 2, 106–108. In Russian.

Panina, L.I., Usoltseva, L.M., 2000. The role of liquid immiscibility of calcitic carbonatites from the Malyi Murun Massif (Aldan). Geology and Geophysics 41, 655–670.

Prokofiev, V.Y., Vorobiev, E.I., 1991. P-T conditions of formation of the Sr-Ba carbonatites, charoite rocks and torgolites of the Murunsky alkaline complex (Eastern Siberia). Geochemistry 10, 1444–1452. In Russian.

Reguir, E., 2001. Aspects of the Mineralogy of the Murun Alkaline Complex, Yakutia, Russia. Lakehead University. Department of geology, Ontario, Canada. PhD thesis.

Robins, B., Furnes, H., Ryan, P., 1983. A new occurrence of dalyite. Mineralogical Magazine 47 (342), 93–94.

Rogov, Y.G., Rogova, V.P., Voronkov, A.A., Moleva, V.A., 1965. Tinaksite, $NaK_2Ca_2TiSi_7O_{19}(OH)$ - a new mineral. Doklady Akademii Nauk USSR 162, 658–661. In Russian.

Rogova, V.P., 1982. Charoitization as a new type of metasomatic processes. In: In ProceedIngs of the All-Soviet MeetIng on Metasomatose. VSEGEI, pp. 113–118. In Russian.

Rogova, V.P., and Sidorenko, G.A., 1964. The find of wadeite in intrusive leycitic rocks of the Murun complex. (G.P. Barsanov, Ed.) Proceedings of the Fersman Mineralogical Museum, Soviet Academy of Sciences, 15, 1–7 (In Russian).

Rogova, V.P., Rogov, Y.G., Drits, V.A., Kuznetsova, N.I., 1978. Charoite - a new mineral and new jewelry-stone. Zapiski Vsesoyuznogo Mineralogicheskogo Obshchestva 1, 94–100. In Russian.

Rubatto, D., 2002. Zircon trace element geochemistry: Partitioning with garnet and the link between U-Pb ages and metamorphism. Chemical Geology 184 (1-2), 123–138.

Rubatto, D., Hermann, J., 2007. Experimental zircon/melt and zircon/garnet trace element partitioning and implications for the geochronology of crustal rocks. Chemical Geology 241 (1-2), 38–61.

Salvi, S., Williams-Jones, A.E., 1995. Zirconosilicate phase relations in the Strange Lake (Lac Brisson) pluton, Quebec-Labrador, Canada. American Mineralogist 80 (9-10), 1031–1040.

Schingaro, E., Mesto, E., Lacalamita, M., Scordari, F., Kaneva, E., Vladykin, F.N., 2017. Single-crystal X-ray diffraction, EMPA, FTIR and X-ray photoelectron spectroscopy study of narsarsukite from Murun Massif, Russia. Mineralogical Magazine 81 (2), 339–354.

Stepanov, A.S., Hermann, J., Rubatto, D., Korsakov, A.V., Danyushevsky, L., 2016. Melting history of an ultrahigh-pressure paragneiss revealed by multiphase solid inclusions in garnet, Kokchetav Massif, Kazakhstan. Journal of Petrology 57, 1531–1554.

Van Tassel, R., Hey, M.H., 1952. Dalyite, a new potassium zirconium silicate, from Ascension Island, Atlantic. Mineralogical Magazine 29 (217), 850–857.

Vladykin, N.V., 2005. Unique Murun complex of ultrapotassic agpaitic alkaline rocks and carbonatites - magmatism and genesis. Applied Geochemistry 7, 124–143.

Vladykin, N.V., 2009. Potassium alkaline lamproite-carbonatite complexes: Petrology, genesis, and ore reserves. Russian Geology and Geophysics 50, 1119–1128.

Vladykin, N.V., 2016. Genesis and crystallization of ultramafic alkaline carbonatite magmas of Siberia, ore-potential, mantle sources and relationship with plume activity. Russian Geology and Geophysics 57, 698–712.

Vladykin, N.V., Borovikov, A.A., Dokuchits, E.Y., Tomas, V.G., 2018. Genesis of charoite rocks of the Murun massif, Aldan shield, Russia. Geochemistry International 56, 1135–1147.

Vladykin, N.V., Matveeva, L.N., Bogacheva, N.G., and Alekseev, Y.A., 1983. New data on charoite and charoitic rocks. In Mineralogy and genesis of precious stones of the Eastern Siberia pp. 41–56. Novosibirsk (In Russian).

Vladykin, N.V., Simonov, V.A., and Sokolov, S.V., 1994. Fluid regime and crystallization temperatures of minerals of charoitic rocks. In Scientific Proceedings Vol. 3, pp. 76–82. Institute of Geology, Geophysics and Mineralogy SB RAS, Novosibirsk (In Russian).

Vladykin, N.V., Tsaruk, I.I., 2003. Geology, chemistry, and genesis of Ba-Sr-bearing ("benstonite") carbonatites of the Murun Massif. Geology and Geophysics 44, 325–339.

Vorobiev, E.I., 2001. Strontium-barium carbonatites of the Murun massif (Eastern Siberia, Russia). Geology of Ore Deposits 43, 468–480.

Vorobiev, E.I., Malyshonok, Yu.V., and Alekseev, Y.A., 1983. To a genesis of charoite. In Problems of crystallochemistry and genesis of minerals pp. 83–93. Nedra (In Russian).
Vorobiev, E.I., 2008. Charoite, 140 p. (L.D. Zorina, Ed.). Geo Publishing House, Novosibirsk (In Russian).
Wang, Y., He, H., Ivanov, A.V., Zhu, R., Lo, C., 2014. Age and origin of charoitite, Malyy Murun massif, Siberia, Russia. International Geology Review 56 (8), 1007–1019.
Wark, D.A., Watson, E.B., 2006. TitaniQ: a titanium-in-quartz geothermometer. Contributions to Mineralogy and Petrology 152 (6), 743–754.
Warr, L.N., 2021. IMA–CNMNC approved mineral symbols. Mineralogical Magazine 85 (3), 291–320.
Watson, E.B., Wark, D.A., Thomas, J.B., 2006. Crystallization thermometers for zircon and rutile. Contributions to Mineralogy and Petrology 151 (4), 413–433.
Yang, S.-Y., Jiang, S.-Y., Mao, Q., Chen, Z.-Y., Rao, C., Li, X.-L., Li, W.-C., Yang, W.-Q., He, P.-L., Li, X., 2022. Electron probe microanalysis in geosciences: Analytical procedures and recent advances. Atomic Spectroscopy 43, 186–200.
Zack, T., Moraes, R., Kronz, A., 2004. Temperature dependence of Zr in rutile: Empirical calibration of a rutile thermometer. Contributions to Mineralogy and Petrology 148, 471–488.
Zhang, R.-X., Yang, S.-Y., 2016. A mathematical model for determining carbon coating thickness and its application in electron probe microanalysis. Microscopy and Microanalysis 22, 1374–1380.
Zhukova, I.A., Stepanov, A.S., Jiang, S.-Y., Murphy, D.T., Mavrogenes, J.A., Chen, W., Bottrill, R., 2021. Complex REE systematics of carbonatites and weathering products from uniquely rich Mount Weld REE deposit, Western Australia. Ore Geology Reviews 139.